Journal of Statistical Mechanics:
Theory and Experiment

STOCHASTIC THERMODYNAMICS

Interlacing relaxation and first-passage phenomena in reversible discrete and continuous space Markovian dynamics

Journal of Statistical Mechanics: Theory and Experiment
An IOP and SISSA journal

Interlacing relaxation and first-passage phenomena in reversible discrete and continuous space Markovian dynamics

David Hartich and Aljaž Godec

Mathematical Biophysics Group, Max-Planck-Institute for Biophysical Chemistry, Göttingen 37077, Germany
E-mail: david.hartich@mpibpc.mpg.de and agodec@mpibpc.mpg.de

Received 23 October 2018
Accepted for publication 27 December 2018
Published 25 February 2019

Online at stacks.iop.org/JSTAT/2019/024002
https://doi.org/10.1088/1742-5468/ab00df

Abstract. We uncover a duality between relaxation and first passage processes in ergodic reversible Markovian dynamics in both discrete and continuous state-space. The duality exists in the form of a spectral interlacing—the respective time scales of relaxation and first passage are shown to interlace. Our canonical theory allows for the first time to determine the full first passage time distribution analytically from the simpler relaxation eigenspectrum. The duality is derived and proven rigorously for both discrete state Markov processes in arbitrary dimension and effectively one-dimensional diffusion processes, whereas we also discuss extensions to more complex scenarios. We apply our theory to a simple discrete-state protein folding model and to the Ornstein–Uhlenbeck process, for which we obtain the exact first passage time distribution analytically in terms of a Newton series of determinants of almost triangular matrices.

Keywords: exact results, stochastic processes, stochastic search, fluctuation phenomena

J. Stat. Mech. (2019) 024002

1742-5468/19/024002+28$33.00

Contents

1. Introduction

In his seminal work [1] Kramers analyzed the kinetics of chemical reactions in terms of diffusive barrier crossing, assuming that the kinetic rate of a chemical reaction corresponds to the inverse of the mean first crossing time. Ever since, first passage theory is at the heart of theoretical descriptions of kinetics of chemical reactions [2–7]; see e.g. [8–11] for comprehensive reviews.

In a broader context, first passage concepts were invoked in studies of kinetics in complex media, such as reactions in fractal-like [12, 13] and planar domains [14, 15], in inhomogeneous cellular environments [16–19], in the study of neural networks [20, 21], ultra cold atoms [22], as well as in diverse narrow escape problems [23–28] and so-called intermittent search strategies involving searching agents with internal dynamics [29, 30] (see also [31] for a review).

https://doi.org/10.1088/1742-5468/ab00df

J. Stat. Mech. (2019) 024002

First passage times play an important role in quantifying persistence properties in non-equilibrium interacting many-body systems [32–34]. More recent applications of first passage concepts also include stochastic thermodynamics [35–37], in particular, fluctuation relations for stopping time statistics and stochastic entropy production in driven molecular systems [38] and in stochastic resetting processes [39, 40], as well as uncertainty relations for first passage time statistics of fluctuating currents [41, 42] (see also [43]).

Moreover, our current understanding of the speed and precision of transcription regulation in biological cells, and in particular of the role of the so-called proximity effect in the co-regulation of genes, [44, 45] builds on first passage time ideas. The corresponding physical principles underlying these proximity effects were explained in [46–48]. Notably, these works revealed the inherent insufficiency of the mean first passage time and traditional rate-based concepts for a quantitative description of biophysical dynamics in the so-called few encounter limit [48]. As a result, a quantitative understanding of phenomena such as gene regulation [44–50] and the misfolding-triggered pathological aggregation of proteins [51–56], which are discussed in more detail in a related study [57], requires the consideration of the full statistics of first passage time.

Existing studies of the full first passage statistics in physical systems typically focus on systems with continuous state-space dynamics, whereas much less emphasis is put on discrete-space dynamics [58]. Recent investigations of such discrete-state dynamics include, for example, simple models of enzyme kinetics [59–61] and novel numerical approximation schemes for studying first-passage statistics based on Bayesian inference [62] (see also [63] for a recent review).

Complementary to first passage processes are relaxation dynamics, which by contrast do not terminate upon reaching a given threshold for the first time. Relaxation phenomena in reversible diffusive dynamical systems are nowadays well understood in terms of the eigenmodes and eigenvalues of the underlying Fokker–Planck operators, which provide a generic and very intuitive understanding of the dynamics of complex stochastic systems [64–66]. Conversely, despite for allowing an analogous spectral representation, a similar intuitive understanding of the full first passage statistics and its physical implications remains elusive. Notwithstanding, an important approximate link between the mean first passage time for escaping the deepest potential basin and the corresponding slowest relaxation mode in the potential was established in the seminal works of Matkovsky and Schuss [67, 68], which has ever since been used routinely in explaining relaxation phenomena in condensed matter systems. Nevertheless, a deeper and more generic connection between the two paradigms to date was not yet established.

Here, we present the complete duality between relaxation and first passage phenomena, which holds for all ergodic Markov processes obeying detailed balance in both, continuous and discrete state-space, in which the absorbing target is effectively 1D. The duality emerges in the form of a spectral interlacing, which we prove rigorously by combining spectral-theoretic, matrix-algebraic and Greens function-theoretic concepts. On the one hand the duality allows for an intuitive generic understanding of first passage phenomena in terms of relaxation eigenmodes. On the other hand, it enables us to determine the full first passage time statistics exactly from the corresponding relaxation eigensystem. The formalism is exact and holds for all reversible Markovian systems

J. Stat. Mech. (2019) 024002

governed by a master equation in arbitrary dimensions or by a Fokker–Planck equation, and therefore unifies the theoretical treatment of discrete and continuous space phenomena. We note the spectral interlacing in the case of a discrete state dynamics has also recently be deduced from a 'lumping' of the state dynamics [69].

To illustrate the predictive power of the formalism in practice, we here predominantly focus on systems with discrete state-space dynamics, whereas continuous space dynamics are treated in more detail in a related study [57]. In particular, we here apply our theory to a simple discrete-state protein folding model and to diffusion in a harmonic potential, also know as the Ornstein–Uhlenbeck process. Notably, we obtain, to the best of our knowledge, for the first time an exact analytical solution for the full first passage time distribution of the Ornstein–Uhlenbeck process in the time domain.

The paper is organized as follows. In section 2 we present a canonical formulation the first passage problem applicable to both discrete states-pace and continuous Fokker–Planck dynamics. Sections 3 and 4 provide a step-by-step explanation of how one can exactly determine the first-passage distribution from the corresponding relaxation process, and also contain rigorous proofs of the duality in discrete and continuous state-space dynamics, respectively. We apply the duality framework in section 5 to determine the first passage statistics for a simple protein folding model and for the Ornstein–Uhlenbeck process. A concluding perspective is provided in section 6. In the appendix we derive a compact representation of the long-time asymptotics of the first passage time distribution, which *inter alia* extends our results for the long time asymptotics from equilibrium systems to irreversibly driven systems.

2. Fundamentals

2.1. Relaxation and first passage

We assume that the probability density to find the system in state x at time t upon evolving from an initial state x_0 according to microscopically reversible dynamics, $P(x,t|x_0)$, is governed by

$$\partial_t P(x,t|x_0) = \mathbf{L}P(x,t|x_0), \tag{1}$$

where $\mathbf{L}$ is a linear reversible operator, which will be specified below. We consider two classes of operators: (DS) discrete state Markov jump process, where x and x_0 assume only a finite number of states, and (FP) continuous Markovian diffusion governed by a Fokker–Planck equation.

For discrete Markov state models of class the dynamics is governed by

$$\mathbf{L}P(x,t|x_0) \equiv \sum_{x'=0}^{M} L(x,x')P(x',t|x_0), \tag{2}$$

where $x, x' = 0, 1, \ldots, M$ denote the discrete states, $L(x,x')$ is the rate of jumping from state x' to state x ($x \neq x'$) and $-L(x,x) = \sum_{x' \neq x} L(x',x)$ is the total rate of leaving state x guaranteeing conservation of probability ($\sum_x \partial_t P(x,t|x_0) = 0$). In order to have reversible dynamics we need to additionally impose detailed balance, i.e. the

J. Stat. Mech. (2019) 024002

constraint $L(x,x')/L(x',x) = \exp[\beta U(x') - \beta U(x)]$ (see., e.g. [70]), which assures that the system will relax to a Boltzmann distribution in a potential $U(x)$ on ergodic timescales $P_{\rm eq}(x) \propto {\rm e}^{-\beta U(x)}$, where $\beta = 1/k_{\rm B}T$ is the inverse thermal energy. We call such a reversible ergodic process that conserves probability a *relaxation process*. If we add an absorbing point at $x = a$ we call the resulting process a *first passage process* or in short absorption, which we introduce in the following way. First, we modify the generator ($\mathbf{L} \to \mathbf{L}_a$) such that all transitions corresponding to jumps out of the absorbing state a are removed, i.e. the elements of the first passage generator read

$$L_a(x,x') = \begin{cases} 0 & \text{if } x' = a, \\ L(x,x') & \text{otherwise.} \end{cases} \tag{3}$$

Using a bra-ket matrix notation [71] we rewrite this equation as

$$\mathbf{L}_a = \mathbf{L} - \mathbf{L}|a\rangle\langle a|, \tag{4}$$

where $|a\rangle = (0,\ldots,0,1,0,\ldots,0)^{\top} = (|a\rangle)^{\top}$ is a vector with all entries except the ath one; consequently, we identify $L_a(x,x') = \langle x|\mathbf{L}_a|x'\rangle$. The first passage time density to reach state a at time t starting from x_0 is then formally defined by

$$\wp_a(t|x_0) = \partial_t \langle a|{\rm e}^{\mathbf{L}_a t}|x_0\rangle = \langle a|\mathbf{L}_a {\rm e}^{\mathbf{L}_a t}|x_0\rangle, \tag{5}$$

which is nothing but the normalized probability flux into state a with $\int_0^\infty \wp_a(t|x_0){\rm d}t = 1$. Note that with equation (4) we use the convention that $|a\rangle$ is the unique stationary solution with $\mathbf{L}_a|a\rangle = 0$.

For a continuous space Markovian diffusion the transition probability density function (the 'propagator') instead obeys the Fokker–Planck equation (1)

$$\begin{aligned} \mathbf{L}P(x,t|x_0) &= -\partial_x j(x,t|x_0) \\ &\equiv \partial_x D[\beta U'(x) + \partial_x]P(x,t|x_0), \end{aligned} \tag{6}$$

where $j(x,t|x_0)$ is the probability current, D is the diffusion constant, $-U'(x) = -\partial_x U(x)$ is a force field generated by the potential $U(x)$ at position x, and β is the inverse temperature, which we set to $\beta \equiv 1$ to express energies in units of $k_{\rm B}T$ from now on. The scenario with reflecting barriers at $x = b_\pm$ with $j(b_\pm,t|x_0) = 0$ [9], we term a *relaxation process*, where $b_\pm = \pm\infty$ correspond to so-called natural boundary conditions[1].

Conversely, an absorbing boundary at $x = a$ enters the Fokker–Planck equation via the Dirichlet boundary condition $P(a,t|x_0) = 0$, without altering the partial differential equation (6), i.e. the first passage operator still reads $\mathbf{L}_a = \partial_x D[U'(x) + \partial_x]$. However, here the first passage time density becomes the probability flux into state a. For convenience we use the operator $\mathbf{L}_a$ as shorthand for equation (6) under the boundary condition $P(a,t|x_0) = 0$.

We note that without an absorbing point both, dynamics governed by the master equation (2) and the Fokker–Planck equation (6) relax to the Boltzmann distribution $P_{\rm eq}(x) \propto \exp[-U(x)]$, whereas with the absorbing boundary condition the particle will eventually reach the target with probability 1.

[1] For natural boundary conditions the current and the probability density both vanish, i.e. $\lim_{b\to\pm\infty} j(b,t|x_0) = \lim_{b\to\pm\infty} P(b,t|x_0) = 0$.

J. Stat. Mech. (2019) 024002

2.2. Eigendecomposition

Since $\mathbf{L}$ is assumed to generate a reversible Markov process, we can expand the generator $\mathbf{L}$ in a bi-orthogonal eigenbasis [72]. Denoting the eigenvalues of the relaxation process by λ_k and the corresponding left (right) eigenvectors by $\langle\psi_k^{\mathrm{L}}|$ ($|\psi_k^{\mathrm{R}}\rangle$), respectively, the generators from equations (2) and (6) become in the respective eigenbases

$$\mathbf{L} = -\sum_k \lambda_k |\psi_k^{\mathrm{R}}\rangle\langle\psi_k^{\mathrm{L}}|, \tag{7}$$

where $\lambda_0 = 0 \leqslant \lambda_1 \leqslant \ldots$, and $\langle\psi_k^{\mathrm{L}}|\psi_l^{\mathrm{R}}\rangle = \delta_{kl}$. We assume the eigenvalues to be ordered such that $\lambda_k \leqslant \lambda_{k+1}$, and the generator to be irreducible $\lambda_0 = 0 < \lambda_1$, which means that there is a unique equilibrium state [70]. Note that for a Fokker–Planck equation with reflecting barriers at $x = b_\pm$ (relaxation) the eigenfunction $\psi_k^{\mathrm{R}}(x) \equiv \langle x|\psi_k^{\mathrm{R}}\rangle$ must satisfy the zero flux condition $-D[U'(x) + \partial_x]\psi_k^{\mathrm{R}}(x)|_{x=b_\pm} = 0$, with $\langle x|\psi_0^{\mathrm{R}}\rangle \propto \mathrm{e}^{-U(x)}$.

The generator with the absorbing point at state a, can similarly be expanded in a bi-orthogonal set of eigenfunctions

$$\mathbf{L}_a = -\sum_k \mu_k |\phi_k^{\mathrm{R}}\rangle\langle\phi_k^{\mathrm{L}}|, \tag{8}$$

where μ_k is the kth eigenvalue and $\langle\phi_k^{\mathrm{L}}|$ ($|\phi_k^{\mathrm{R}}\rangle$) denote the corresponding left (right) eigenfunctions of the first passage process. Without loss generality we use an ordered labeling such that $\mu_k \leqslant \mu_{k+1}$, where $0 < \mu_1$.

The left and right eigenvectors of the absorption (at position $x \neq a$) as well as of the relaxation process are related via $\langle x|\phi_k^{\mathrm{L}}\rangle \propto \mathrm{e}^{U(x)}\langle x|\phi_k^{\mathrm{R}}\rangle$ and $\langle x|\psi_k^{\mathrm{L}}\rangle \propto \mathrm{e}^{U(x)}\langle x|\psi_k^{\mathrm{R}}\rangle$, respectively. In the case of a discrete number of states, the lowest eigenvalue of the generator (4) will be $\mu_0 = 0$ with the right eigenfunction $|\phi_0^{\mathrm{R}}\rangle = |a\rangle$, whereas for Fokker–Planck dynamics one imposes the boundary condition $\langle a|\phi_k^{\mathrm{R}}\rangle = 0$.

In a previous work an explicit Newton series expression for μ_1 in terms of a series of almost triangular matrices was derived [48], which corresponds to a large deviation limit $t \to \infty$. One of our main goals here is to obtain the full first passage statistics $\wp_a(t|x_0)$ explicitly in terms of relaxation eigenmodes. Our theory builds on the renewal theorem, which we briefly review in the following subsection.

2.3. Renewal theorem

The classical renewal theorem provides a well known implicit connection between first passage and relaxation processes. It relates the probability density of the freely propagating system to be in state x at time t upon starting from a state x_0, to the first passage distribution $\wp_a(t|x_0)$ from x_0 to a:

$$P(x,t|x_0) = \int_0^t \mathrm{d}\tau P(x,t-\tau|a)\wp_a(\tau|x_0), \tag{9}$$

where both $P(x,t|x_0)$ and $\wp_a(t|x_0)$ admit a spectral representation

$$P(x,t|x_0) = \langle x|\mathrm{e}^{\mathbf{L}t}|x_0\rangle = \sum_k \langle x|\psi_k^{\mathrm{R}}\rangle\langle\psi_k^{\mathrm{L}}|x_0\rangle \mathrm{e}^{-\lambda_k t} \tag{10}$$

J. Stat. Mech. (2019) 024002

and

$$\wp_a(t|x_0) = \sum_{k\geqslant 1} w_k(x_0)\mu_k \mathrm{e}^{-\mu_k t}, \tag{11}$$

respectively. In other words, a system starting from state x_0 must pass through state a before reaching the final state x, which for an effectively 1D Fokker–Planck necessarily means $x_0 < a \leqslant x$ or $x_0 > a \geqslant x$. In equation (11) we introduced in the first passage weights

$$w_k(x_0) = \begin{cases} -\langle a|\phi_k^{\mathrm{R}}\rangle\langle\phi_k^{\mathrm{L}}|x_0\rangle & \text{for DS,} \\ -\sigma_\pm D \frac{\partial\langle x|\phi_k^{\mathrm{R}}\rangle}{\partial x}\Big|_{x=a} \frac{\langle\phi_k^{\mathrm{L}}|x_0\rangle}{\mu_k} & \text{for FP,} \end{cases} \tag{12}$$

for DS and FP dynamics, respectively, which must satisfy $\sum_k w_k = 1$ with the first nonzero weight being strictly positive $w_1(x_0) > 0$, and where we introduced $\sigma_\pm \equiv \mathrm{sign}(a - x_0)$. Note that the first line of equation (12), i.e. the DS case, is equivalent to $w_k(x_0) = \sum_{x\neq a}\langle x|\phi_k^{\mathrm{R}}\rangle\langle\phi_k^{\mathrm{L}}|x_0\rangle$ with $\mathbf{L}_a$ from equation (4). In the case of FP dynamics the second line of equation (12) is equivalent to $w_k(x_0) \equiv \int\langle x|\phi_k^{\mathrm{R}}\rangle\langle\phi_k^{\mathrm{L}}|x_0\rangle \mathrm{d}x$, which follows from a partial integration using both equations (6) and (8).

In the case of $x = a$ the renewal theorem (9) has the simple interpretation: a system being in state a at time t must have arrived at that point at some earlier time τ for the first time ($\tau \leqslant t$), and then returned to the same position again at time t, where $\tau = t$ corresponds to the time of first arrival.

Laplace transforming the renewal theorem (9), where a generic function f is transformed according to $\tilde{f}(s) \equiv \int \mathrm{e}^{-st} f(t)\mathrm{d}t$, yields [73]

$$\tilde{\wp}_a(s|x_0) = \frac{\tilde{P}(x,s|x_0)}{\tilde{P}(x,s|a)} = \frac{\sum_k (s+\lambda_k)^{-1}\langle x|\psi_k^{\mathrm{R}}\rangle\langle\psi_k^{\mathrm{L}}|x_0\rangle}{\sum_k (s+\lambda_k)^{-1}\langle x|\psi_k^{\mathrm{R}}\rangle\langle\psi_k^{\mathrm{L}}|a\rangle}. \tag{13}$$

Based on this well known renewal theorem we construct in the following section a method that allows to determine explicitly the first passage time statistics $\wp_a(t|x_0)$ exactly in terms of the relaxation process, i.e. we render equation (13) explicit in the time domain.

3. Principal result for discrete state systems

Starting from the renewal theorem (13), we now derive an expression for the first passage time density for discrete state Markov processes in terms of relaxation modes in the following three steps. The first step involves a crucial relation between the eigenvalues of the relaxation process λ_k and absorption process μ_k, which are here shown to interlace

$$\lambda_{k-1} \leqslant \mu_k \leqslant \lambda_k \tag{14}$$

for $k = 1, \ldots, M$. For effectively one dimensional finite lattice models with the target at an outer edge these inequalities become strict

J. Stat. Mech. (2019) 024002

$$\lambda_{k-1} < \mu_k < \lambda_k, \tag{15}$$

which will also apply identically to Fokker–Planck dynamics discussed in section 4 in which case we formally assume $M = \infty$. In the second step we exactly express the first passage eigenvalues μ_k in the form of a Newton series of determinants of almost triangular matrices, which generalizes the result for the slowest mode μ_1 from [48] to all first passage modes. The third and final step corresponds to a straightforward application of the residue theorem, which is used to determine the first passage weights $w_k(x_0)$.

3.1. Interlacing of eigenmodes (step 1)

For a discrete system with $M+1$ states the eigenvalues λ_k and μ_k correspond to the roots of the respective characteristic polynomials

$$\begin{aligned} \chi(s) &\equiv \det(1s - \mathbf{L}) = s\prod_{i=1}^{M}(s+\lambda_i), \\ \chi_a(s) &\equiv \det(1s - \mathbf{L}_a) = s\prod_{i=1}^{M}(s+\mu_i), \end{aligned} \tag{16}$$

i.e. $\chi(-\lambda_k) = 0$ and $\chi_a(-\mu_k) = 0$. Inserting equation (4), which is $\mathbf{L}_a = \mathbf{L} - \mathbf{L}|a\rangle\langle a|$, into the second characteristic polynomial (16) and using the matrix determinant lemma establishes a link between the two characteristic polynomials

$$\chi_a(s) = \chi(s) + \langle a|\mathrm{adj}(1s - \mathbf{L})\mathbf{L}|a\rangle, \tag{17}$$

where $\mathrm{adj}(\mathbf{A})$ is called the adjugate of a matrix $\mathbf{A}$ satisfying Cramer's rule $\mathbf{A}\mathrm{adj}(\mathbf{A}) = \det(\mathbf{A})1$. We note that the same mathematical concepts have been used recently to determine the stalling distribution of irreversibly driven systems (see deletion-contraction formula in [74, 75]).

The adjugate of a diagonal matrix $\mathbf{D}$ with elements $D_{ii} = d_i$ ($D_{ij} = 0$ if $i \neq j$) is diagonal as well, with elements $\mathrm{adj}(\mathbf{D})_{ii} = \prod_{j\neq i} d_j$. Consequently, the bi-orthogonal expansion (7) implies

$$\mathrm{adj}(1s - \mathbf{L}) = \sum_{i=0}^{M} |\psi_i^{\mathrm{R}}\rangle\langle\psi_i^{\mathrm{L}}| \prod_{\substack{j=0 \\ j\neq i}}^{M}(s+\lambda_j), \tag{18}$$

which inserted into equation (17) gives

$$\chi_a(s) = \chi(s) - \sum_{i=0}^{M}\langle a|\psi_i^{\mathrm{R}}\rangle\langle\psi_i^{\mathrm{L}}|a\rangle\lambda_i \prod_{\substack{j=0 \\ j\neq i}}^{M}(s+\lambda_j), \tag{19}$$

where we used the eigenvalue equation $\langle\psi_i^{\mathrm{L}}|\mathbf{L}|a\rangle = -\lambda_i\langle\psi_i^{\mathrm{L}}|a\rangle$. Equation (19) constitutes an essential step in our calculations, which allows us to express the diagonal of the relaxation propagator $\tilde{P}(a, s|a)$ solely in terms of eigenvalues μ_k and λ_k (see the following subsection for more details).

Moreover, the characteristic polynomials of the first passage process $\chi_a(s)$ and relaxation process $\chi(s)$ change sign one after the other, since detailed balance imposes

J. Stat. Mech. (2019) 024002

$\langle a|\psi_i^{\mathrm{R}}\rangle\langle\psi_i^{\mathrm{L}}|a\rangle \geqslant 0$ for all $i = 0, \ldots, M$, which proves that the eigenvalues of the first passage process μ_k and eigenvalues of the relaxation process λ_k interlace according to equation (14). We note that this result is directly related to the interlacing of eigenvalues generated from a 'lumping' of states which is proven in [69]. In the following paragraph we briefly discuss the scenario, in which the interlacing of eigenvalues becomes strict (15), which will be the case for systems with Fokker–Planck dynamics discussed in section 4.2.

The stronger condition (15) holds if all eigenfunctions are nonzero at the target $|\langle a|\psi_k^{\mathrm{R}}\rangle| > 0$ and all relaxation eigenvalues are non-degenerate, that is, $\lambda_{i-1} < \lambda_i$ for all $i = 1, \ldots, M$. One can show that this condition is always trivially satisfied for 1D models ($L(x, x') = 0$ if $|x - x'| > 1$), in which the target a is placed at the border (e.g. $a = M$ or $a = 0$); see inset of figure 1(a) for such an exemplary three-state system.

Inserting the relaxation eigenvalues $s = -\lambda_k$ into the characteristic polynomial of the first passage process (19) yields

$$\chi_a(-\lambda_k) = (-1)^{k+1}\lambda_k\langle a|\psi_i^{\mathrm{R}}\rangle\langle\psi_i^{\mathrm{L}}|a\rangle\prod_{\substack{i=0\\ i\neq k}}^{M}|\lambda_i - \lambda_k|, \tag{20}$$

where we used the relations $\lambda_i - \lambda_k < 0$ for all $i < k$ and $\lambda_i - \lambda_k > 0$ for all $i > k$, as well as $\chi(-\lambda_k) = 0$. Since for $k \geqslant 1$ each eigenvalue is positive ($\lambda_k > 0$), the characteristic polynomial of the first passage process $\chi_a(-\lambda_k)$ is equal to $(-1)^{k-1}$ multiplied by a positive constant. Consequently, χ_a changes sign exactly once between any two consecutive relaxation modes $-\lambda_k < s < -\lambda_{k-1}$. The fact that χ_a and χ are polynomials of the same degree $M + 1$ forbids more than a single root, and hence implies the strict interlacing of eigenvalues from equation (15), which completes the proof. The aforementioned reasoning is illustrated in figure 1(a) for a simple three state model in which the vertical arrows represent equation (20).

For fine-tuned systems in which the target is not located at the very outer position (see e.g. figure 1(b)) or systems that are not effectively one dimensional (see e.g. figure 1(c)) the strict interlacing theorem (15) can be violated, whereas the 'slightly weaker' interlacing condition (14) still holds.

3.2. Diagonal of the relaxation propagator in terms of bare eigenvalues

Using the results from the previous subsection we are now in the position to represent $\tilde{P}(a, s|a)$ (i.e. equation (10) with $x_0 = x = a$), using only the eigenvalues of both the first passage process and the relaxation process, μ_k and λ_k, respectively. Laplace transforming the eigenmode expansion in equation (10) assuming $x_0 = x = a$ yields

$$\tilde{P}(a, s|a) = \frac{P_{\mathrm{eq}}(a)}{s} + \sum_{k=1}^{M}\frac{\langle a|\psi_k^{\mathrm{R}}\rangle\langle\psi_k^{\mathrm{L}}|a\rangle}{s + \lambda_k}, \tag{21}$$

where we identified the equilibrium probability density $\langle a|\psi_0^{\mathrm{R}}\rangle\langle\psi_0^{\mathrm{L}}|a\rangle = P_{\mathrm{eq}}(a)$ in the first term. Comparing now $\tilde{P}(a, s|a)$ in (21) with χ_a from equation (19) and χ from equation (16) yields after some algebra

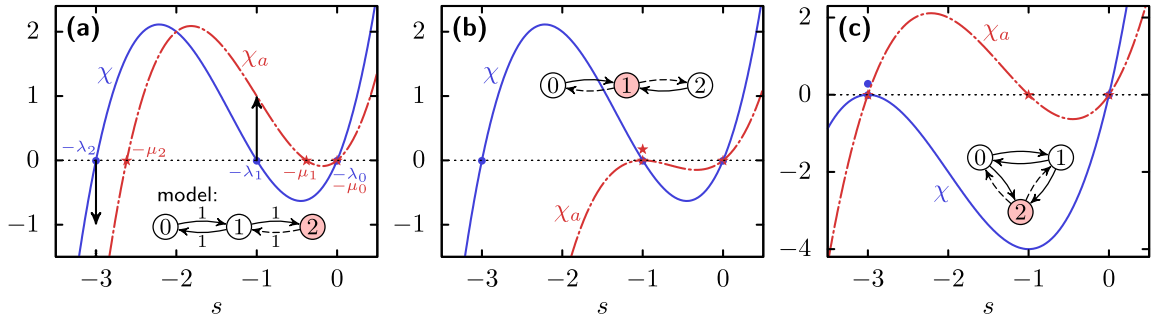

Figure 1. Characteristic polynomials χ (solid blue line) and χ_a (dash-dotted red line) for simple three state models (see insets) along real axis in s. (a) Linear chain of states with the absorbing state at the border $a = 2$. χ crosses the s axis at $s = -3, -1, 0$ which correspond to $-\lambda_2, -\lambda_1, -\lambda_0$, respectively. (b) The same model as in (a) but with the absorbing state at $a = 1$. The first eigenmode $|\psi_1^{\mathrm{R}}\rangle = (1, 0, 1)^{\top}$ vanishes at the target. (c) Fully connected three state model, in which $\lambda_1 = \lambda_2$. All rates in (a)–(c) are set to 1 (relaxation process). The transition rates away from absorbing point (dashed arrows) are set to zero (absorption). We note this special choice of rates deliberately generates a multiplicity of the first relaxation mode in (b) and the first passage mode in (c).

$$\tilde{P}(a, s|a) = \frac{\chi_a(s)}{s\chi(s)} = \frac{1}{s}\prod_{i=1}^{M}\frac{(s+\mu_i)}{(s+\lambda_i)}. \tag{22}$$

The second equality in equation (22) follows from equation (16). Hence, $\tilde{P}(a, s|a)$ encodes the eigenvalues of both, the relaxation and the first passage processes. Due to equation (21) $\tilde{P}(a, s|a)$ contains only simple poles and decreases monotonically in s between any two consecutive poles since $\langle a|\psi_k^{\mathrm{R}}\rangle\langle\psi_k^{\mathrm{L}}|a\rangle \geqslant 0$. If $\langle a|\psi_k^{\mathrm{R}}\rangle\langle\psi_k^{\mathrm{L}}|a\rangle > 0$ (e.g. 1d models with the target at at the border) each root λ_k of $\tilde{P}(a, s|a)$ represents a first passage eigenvalue $s = -\mu_k$ ($k \geqslant 1$), which is located in between two relaxation modes $\lambda_{k-1} < \mu_k < \lambda_k$, thus providing an alternative proof of relation (15) [76]. In the following section we determine the roots of the diagonal of the propagator explicitly, which due to equation (22) correspond to first passage eigenvalues μ_k.

Let us briefly reformulate $\tilde{P}(a, s|a)$ in a way that can also be applied to continuous systems with an infinite number of states. Isolating the equilibrium probability, which is the first term in equation (21), from the product formula (22) yields

$$\tilde{P}(a, s|a) = \frac{P_{\mathrm{eq}}(a)}{s}\prod_{k=1}^{M}\frac{(1+s/\mu_k)}{(1+s/\lambda_k)}. \tag{23}$$

Since μ_k, λ_k increase monotonically with k we will later be able to adopt these results to systems governed by Fokker–Planck dynamics, which formally corresponds to the limit $M \to \infty$ for which the product in equation (23) still converges.

J. Stat. Mech. (2019) 024002

3.3. From the relaxation spectrum to the first passage time spectrum (steps 2 and 3)

Based on the interlacing theorem presented in equation (14), which is also given in equation (4) in a related work [57], we can determine the full first passage time spectrum $\{\mu_k, w_k(x_0)\}$ from the corresponding relaxation spectrum, $\{\lambda_k, |\psi_k^{\mathrm{R}}\rangle, \langle\psi_k^{\mathrm{L}}|\}$. For simplicity we first consider the eigenvalues to be both ordered $\lambda_k < \lambda_{k+1}$ and non-degenerate, and also assume that $\langle a|\psi_k^{\mathrm{R}}\rangle\langle\psi_k^{\mathrm{L}}|a\rangle > 0$ holds for all values of k. The extension to situations with $\langle a|\psi_k^{\mathrm{R}}\rangle\langle\psi_k^{\mathrm{L}}|a\rangle = 0$, which also includes degenerate eigenvalues, for some k is straightforward and will be dealt with at the end of this subsection.

Before determining the weights w_k, we first determine the first passage eigenvalues μ_k, which were shown to be encoded in the roots of $\tilde{P}(a,s|a)$ in equation (22). We introduce the k^*th 'modified diagonal of the propagator'

$$\begin{aligned} F_{k^*}(s) &\equiv (s+\lambda_{k^*})\tilde{P}(a,s|a) \\ &= \langle a|\psi_{k^*}^{\mathrm{R}}\rangle\langle\psi_{k^*}^{\mathrm{L}}|a\rangle + (s+\lambda_{k^*})\sum_{\substack{l=0 \\ l\neq k*}}^{M}\frac{\langle a|\psi_l^{\mathrm{R}}\rangle\langle\psi_l^{\mathrm{L}}|a\rangle}{s+\lambda_i}, \end{aligned} \tag{24}$$

which still encodes all of the first passage eigenvalues $\{\mu_k\}$ according to equation (22), i.e. it has exactly the same roots as $\tilde{P}(a,s|a)$. However, in contrast to $\tilde{P}(a,s|a)$ the modified function $F_{k^*}(s)$ is strictly concave within the interval $-\lambda_{k^*+1} < s < -\lambda_{k^*-1}$, which can easily be confirmed by taking the second derivative and realizing that $\ddot{F}_{k^*}(s) \equiv \partial_s^2 F_{k^*}(s) < 0$ holds within the region of interest $-\lambda_{k^*+1} < s < -\lambda_{k^*-1}$.

For $k^* = k$ and $k^* = k-1$ the modified functions $F_k(s)$ and $F_{k-1}(s)$ both are strictly concave within the interval $-\lambda_k < s < -\lambda_{k-1}$ and, consequently, also locally concave around the kth first passage eigenvalue $s = -\mu_k$, i.e. $\ddot{F}_k(-\mu_k)$ and $\ddot{F}_{k-1}(-\mu_k) < 0$. Moreover, both functions $F_k(s)$ and $F_{k-1}(s)$ allow a Taylor expansion around the midpoint $\bar{\mu}_k \equiv (\lambda_k + \lambda_{k-1})/2$ that converges within the whole interval $-\lambda_k < s < -\lambda_{k-1}$ including the root $s = -\mu_k$ at which $F_k(-\mu_k) = F_{k-1}(-\mu_k) = 0$.

The method we present in the following is an analytical technique based on the principles of Newton iteration, which is a simple root finding algorithm that is guaranteed to work for functions that are both negative and concave between the starting point and the first root. Hence, to determine the kth eigenvalue we accordingly choose the modified function

$$f(s,k) = F_{k^*}(s), \tag{25}$$

such that

$$k^* = \begin{cases} k & \text{if } F_k(-\bar{\mu}_k) < 0, \\ k-1 & \text{otherwise.} \end{cases}, \tag{26}$$

which guarantees both negativity $f(s,k) \leqslant 0$ and concavity $\partial_s^2 f(s,k) \leqslant 0$ between $s = -\bar{\mu}_k$ and $s = -\mu_k$.

According to the interlacing theorem (15) $s = -\mu_k$ is the only zero $f(-\mu_k, k) = 0$ within the interval $-\lambda_k < s < -\lambda_{k-1}$. With the midpoint starting condition $\bar{\mu}_k = (\lambda_k + \lambda_{k-1})/2$ the kth first passage eigenvalue can be represented exactly in a series of determinants of almost triangular matrices

J. Stat. Mech. (2019) 024002

$$\mu_k = \bar{\mu}_k + \sum_{n=1}^{\infty} \frac{f_0(k)^n}{f_1(k)^{2n-1}} \frac{\det \boldsymbol{\mathcal{A}}_n(k)}{(n-1)!}, \tag{27}$$

where $f_n(k)$ is the nth derivative of $f(s,k)$ as defined in (25) with respect to s at $s=-\bar{\mu}_k$, and $\boldsymbol{\mathcal{A}}_n(k)$ stands for an almost triangular matrix with elements [48]

$$\boldsymbol{\mathcal{A}}_n^{i,j}(k) = \frac{f_{i-j+2}(k)\Theta(i-j+1)}{(i-j+2)!}\Big[n(i-j+1)\Theta(j-2) + i\Theta(1-j) + j - 1\Big], \tag{28}$$

with $\Theta(l)$ denoting the Heaviside step function ($\Theta(l)=1$ if $l \geqslant 0$) and $i,j = 1,2,\ldots,n-1$. Moreover, we adopt the convention $\det \boldsymbol{\mathcal{A}}_1(k) = 1$. We note that this method generalizes the method recently derived to determine the slowest first passage mode μ_1 [48] to all first passage eigenmodes μ_k.

Let us briefly repeat the two crucial steps towards equation (27). First, the interlacing theorem (15) guarantees that the Taylor series $f(s,k) = \sum_i f_i(k)(s+\bar{\mu}_k)^i$ around the midpoint $\bar{\mu}_k = (\lambda_k + \lambda_{k-1})/2$ converges in the entire spectral interval $-\lambda_k < s < -\lambda_{k-1}$, which also contains the first passage eigenvalue $s=-\mu_k$. Second, due to $F_{k^*}(s)$ in equations (24)–(26) the function $f(s,k)$ is strictly concave and negative between $s=-\bar{\mu}_k$ and $s=-\mu_k$, which in turn guarantees the convergence of the explicit Newton series (27).

Equations (24)–(26) provide a universal method for determining explicitly first passage eigenvalues from the corresponding relaxation spectrum and constitute the central result of this work. We show in the appendix a simpler derivation of μ_1 as well as a compact approximation of the principal first passage eigenvalue μ_1, which is particularly useful in the case of time scale separation $\mu_1 \ll \lambda_1$ (or $\lambda_1 \ll \lambda_2$). Furthermore, the appendix provides a generalization of the long time asymptotics from systems with reversible dynamics to irreversibly driven systems.

In the following we briefly comment on the practical implementation of the exact result for μ_k to render equations (24)–(27) fully explicit. The weights w_k will be determined afterwards in this subsection. The nth derivative of $F_{k^*}(s)$ with respect to s at $s=-\bar{\mu}_k$, $f_n(k) \equiv \partial_s^n f(s,k)|_{s=-\bar{\mu}_k}$, can be written explicitly as

$$\begin{aligned} f_0(k) &= \langle a|\psi_{k^*}^{\mathrm{R}}\rangle\langle\psi_{k^*}^{\mathrm{L}}|a\rangle + \sum_{l|l\neq k^*}\langle a|\psi_l^{\mathrm{R}}\rangle\langle\psi_l^{\mathrm{L}}|a\rangle\frac{(\bar{\mu}_k-\lambda_{k^*})}{(\bar{\mu}_k-\lambda_l)}, \\ f_{n\geqslant 1}(k) &= n!\sum_{l|l\neq k^*}\langle a|\psi_l^{\mathrm{R}}\rangle\langle\psi_l^{\mathrm{L}}|a\rangle\frac{(\lambda_l-\lambda_{k^*})}{(\bar{\mu}_k-\lambda_l)^{n+1}}, \end{aligned} \tag{29}$$

where $k^*=k$ or $k^*=k-1$ is chosen according to equation (26). Note that condition (26) is equivalent to the condition $f_0(k) \leqslant 0$, implying the first line of equation (29) to be either negative for $k^*=k$ or for $k^*=k-1$, i.e. one has to evaluate the first line of equation (29) for $k^*=k$: if $f_0(k)>0$ one must to change k^* to $k^*=k-1$ and reevaluate $f_0(k)$. Once one has determined $k^*(k)$ and $f_0(k)$ one can proceed with the second line of equation (29) to determine $f_n(k)/n!$ and insert the result in the almost triangular matrix (28). The determinant of almost triangular matrices can be calculated elegantly using the simple recursion relation from [77], see also [78] for an efficient numerical implementation.

J. Stat. Mech. (2019) 024002

Having obtained the first passage eigenvalues, the weights of the first passage time distribution can be calculated using the standard residue theorem. The Laplace transform of the spectral expansion of the first passage time density (11) reads

$$\tilde{\wp}_a(s|x_0) \equiv \sum_k \frac{w_k(x_0)\mu_k}{s+\mu_k}. \tag{30}$$

Using the residue theorem to invert the Laplace transformed renewal theorem (13) yields

$$\begin{aligned} w_k(x_0) &= \frac{\tilde{P}(a,-\mu_k|x_0)}{\mu_k \dot{\tilde{P}}(a,-\mu_k|a)} \\ &= \frac{\sum_l (1-\lambda_l/\mu_k)^{-1}\langle a|\psi_l^{\mathrm{R}}\rangle\langle\psi_l^{\mathrm{L}}|x_0\rangle}{\sum_l (1-\lambda_l/\mu_k)^{-2}\langle a|\psi_l^{\mathrm{R}}\rangle\langle\psi_l^{\mathrm{L}}|a\rangle}, \end{aligned} \tag{31}$$

where $\dot{\tilde{P}}(a,s|a) = \partial_s \tilde{P}(a,s|a)$ is taken at $s=-\mu_k$. The explicit Newton series (27) along with the first passage weights (31) fully characterize the first passage time distribution $\wp_a(t|x_0) = \sum_k w_k(x_0)\mu_k \mathrm{e}^{-\mu_k t}$ in terms of relaxation eigenmodes $\{\lambda_k, \psi_k^{\mathrm{R}}\}$. This completes our third and final step, which allows, for the first time, to analytically deduce first passage time statistics directly from relaxation eigenmodes. We call this relation the explicit *forward duality* between first passage and relaxation. This completes the central result of this paper.

The spectral representation is very useful for determining the moments of the first passage time, $\langle t^n\rangle \equiv \int t^n \wp_a(t|x_0)\mathrm{d}t = n!\sum_k w_k(x_0)\mu_k^{-n}$. Moreover, as explained in more detail in a related work [57], the full spectral expansion is required for a correct explanation of kinetics in the so-called few encounter limit, where N molecules starting from position x_0 are searching for the target at a. The probability density that the first molecule out of N arrives at time t at a for the first time for this case becomes $\wp_a^{(N)}(t|x_0) = N\wp_a(t|x_0)[\int_t^\infty \wp_a(\tau|x_0)]^{N-1}\mathrm{d}\tau$, which can be understood as follows. The probability that the first $N-1$ molecule have not yet reached the target will be given by $[\int_t^\infty \wp_a(\tau|x_0)\mathrm{d}\tau]^{N-1}$, while the Nth particle arrives at a with a rate $\wp_a(t|x_0)$; hence the probability density that any particle out of N molecules arrives at the target for the first time according to $\wp_a^{(N)}(t|x_0)$. Further details of the N-particle problem and in particular the physical implications of the few-encounter limit are discussed in a related study [57].

Let us now briefly generalize the method to systems with degenerate eigenvalues or vanishing relaxation modes. An eigenfunction that vanishes at the target $\langle a|\psi_k^{\mathrm{R}}\rangle = 0$ will have a vanishing spectral weight as a result of equation (31). Hence, 'manually' removing such modes will not affect the first passage time distribution $\wp_a$. Moreover, if a relaxation eigenvalue λ_k is degenerate we define

$$\Psi_k(a,x_0) \equiv \sum_{k'|\lambda_{k'}=\lambda_k} \langle a|\psi_{k'}^{\mathrm{R}}\rangle\langle\psi_{k'}^{\mathrm{L}}|x_0\rangle, \tag{32}$$

and replace $\langle a|\psi_k^{\mathrm{R}}\rangle\langle\psi_k^{\mathrm{L}}|x_0\rangle \to \Psi_k(a,x_0)$ as well as $\langle a|\psi_k^{\mathrm{R}}\rangle\langle\psi_k^{\mathrm{L}}|a\rangle \to \Psi_k(a,a)$ and take the sums in equation (13) over all different values of λ_k. After renumbering all distinct contributing eigenvalues we obtain a strict interlacing (15). Therefore, we can apply

J. Stat. Mech. (2019) 024002

our standard forward duality also to degenerate eigensystems. In the next subsection we will briefly derive a formal *backward duality* after which we reformulate the results from this subsection to continuous Fokker–Planck dynamics.

3.4. Backward duality

In contrast to the explicit *forward duality*, which was presented in the previous subsection, an explicit reverse relation in the time-domain could not be established. In Laplace space, however, the forward duality can be inverted to give a backward duality as follows. Inserting the first passage generator $\mathbf{L}_a = \mathbf{L} - \mathbf{L}|a\rangle\langle a|$ from (4) into the Laplace transform of the propagator $\tilde{P}(a, s|x_0) = \langle a|(1s - \mathbf{L})^{-1}|x_0\rangle$ and using the Sherman–Morrison–Woodbury formula yields

$$\tilde{P}(a, s|x_0) = \frac{\langle a|(1s - \mathbf{L}_a)^{-1}|x_0\rangle}{1 - \langle a|(1s - \mathbf{L}_a)^{-1}\mathbf{L}|a\rangle}. \tag{33}$$

Let us now insert the expression for the first passage time distribution from equation (5), which can be written as $\wp_a(s|x_0) = s\langle a|(1s - \mathbf{L}_a)^{-1}|x_0\rangle$, into equation (33) to obtain

$$\tilde{P}(a, s|x_0) = \frac{\tilde{\wp}_a(s|x_0)/s}{1 - \sum_{x=0}^{M} L(x, a)\tilde{\wp}_a(s|x)/s}, \tag{34}$$

where $L(x, a) = \langle x|\mathbf{L}|a\rangle$ is the generator of the relaxation process. Notably, this is expression corresponds to the *backward duality* and is the formal inverse of the renewal theorem, where $\tilde{\wp}_a(s|x_0)/s$ is the Laplace transform of the cumulative first passage time distribution $\int_0^t \wp_a(\tau|x_0)\mathrm{d}\tau$.

4. Principal result for Fokker–Planck dynamics

4.1. Greens function with natural boundaries

We restrict our discussion to effectively 1D dynamics, which include diffusion in d dimensions in an isotropic potential as discussed in [48], where d may also be fractal. Introducing an absorbing target at position a splits the first passage problem into two cases (I) $x_0 < a$ and (II) $x_0 > a$. Case (I) corresponds to an absorption from the left, and case (II) to an absorption from the right. In the following paragraph we demonstrate that all first passage modes μ_k of both distinct cases (I) and (II) are entirely encoded in $\tilde{P}(a, s|a)$, which allows to formulate the results from section 3.3 also for systems with Fokker–Planck dynamics.

Laplace transforming the Fokker–Planck equation (6) yields

$$(\mathbf{L} - s)\tilde{P}(x, s|x_0) = -\delta(x - x_0) \tag{35}$$

where $\mathbf{L} = -\partial_x D[\beta U'(x) + \partial_x]$ and x_0 is the initial position of the relaxation process. Equation (35) is a inhomogeneous linear differential equation which can be solved using the standard Green's function approach. First, we find the two independent

J. Stat. Mech. (2019) 024002

solutions $v_\pm(x,s)$ of the homogeneous problem $(\mathbf{L}-s)v_\pm(x,s)=0$, where we use the label '−' and '+' for the solution satisfying the left and right boundary condition, respectively. That is, a diffusion process within an interval $b_-<x<b_+$ imposes the probability current $j_\pm(x,s)\equiv -D[\beta U'(x)+\partial_x]v_\pm(x,s)$ to vanish at the boundaries, i.e. $j_\pm(b_\pm,s)=0$. The special case of so-called natural boundary conditions correspond to the limit $\lim_{x\to\pm\infty}v_\pm(x,s)=0$ or analogously $\lim_{x\to\pm\infty}j_\pm(x,s)=0$, that is, $b_\pm=\pm\infty$. The full solution $\tilde{P}(x,s|x_0)$ of (35) is a continuous function in x with a discontinuity of its first derivative at $x=x_0$. Using the scaled Wronskian[2]

$$\begin{aligned} W_s(x) &\equiv D[v_-(x,s)\partial_x v_+(x,s)-v_+(x,s)\partial_x v_-(x,s)],\\ &= v_+(x,s)\,j_-(x,s)-v_-(x,s)\,j_+(x,s)\\ &= \det\begin{pmatrix} v_+(x,s) & v_-(x,s)\\ j_+(x,s) & j_-(x,s)\end{pmatrix} \end{aligned} \tag{36}$$

the propagator, which satisfies the proper jump condition of the first derivative (current function) at $x=x_0$, becomes

$$\tilde{P}(x,s|x_0)=\begin{cases}\frac{v_+(x,s)v_-(x_0,s)}{W_s(x_0)} & \text{if } x_0\leqslant x,\\ \frac{v_-(x,s)v_+(x_0,s)}{W_s(x_0)} & \text{if } x_0\geqslant x.\end{cases} \tag{37}$$

We note that the Wronskian (36) is proportional to the Boltzmann factor (see, e.g. [76]), i.e. $W_s(x)=W_s(x_0)\exp[\beta U(x_0)-\beta U(x)]$. Hence using the renewal theorem (13) and $\tilde{P}(a,s|a)$ as well as $\tilde{P}(a,s|x_0)$ from equation (37) yields the Laplace transform of the first passage time distribution

$$\wp_a(s|x_0)=\mathrm{e}^{\beta U(x_0)-\beta U(a)}\times\begin{cases}\frac{v_-(x_0,s)}{v_-(a,s)} & \text{if } x_0<a,\\ \frac{v_+(x_0,s)}{v_+(a,s)} & \text{if } x_0>a.\end{cases} \tag{38}$$

The two independent functions $v_\pm(x,s)$ are entire functions without any poles in s [79], and in turn encode in their roots all first passage eigenvalues $s=-\mu_k$. In particular v_- encodes all first passage modes from case (I) $x_0<a$, and v_+ encodes all first passage modes from case (II), in which the particle is absorbed from the right $x_0>a$. Due to equation (37) the zeros of $\tilde{P}(a,s|a)$ at $s=-\mu_k$ determine the first passage spectrum. Hence, all results from section 3.3 hold identically for continuous systems as well. However, the sums are here not finite, i.e. $M=\infty$. For example, $\tilde{P}(a,s|a)$ becomes

$$\tilde{P}(a,s|a)=\sum_{l=0}^{\infty}\frac{\psi_l^{\mathrm{L}}(a)\psi_l^{\mathrm{R}}(a)}{s+\lambda_l}, \tag{39}$$

where ψ_l^{R} is the lth right eigenfunction of the Fokker–Planck operator satisfying $\mathbf{L}\psi_l^{\mathrm{R}}(x)=-\lambda_l\psi_l^{\mathrm{R}}(x)$ with the corresponding left eigenfunction $\psi_l^{\mathrm{L}}(a)\propto\mathrm{e}^{\beta U(a)}\psi_l^{\mathrm{R}}(a)$ and normalization $\int_{b_-}^{b_+}\psi_l^{\mathrm{R}}(x)\psi_l^{\mathrm{L}}(x)\mathrm{d}x=1$. The first passage modes μ_k can then be determined with equations (27)–(29), where k^* ($k^*=k$ or $k^*=k-1$) must be chosen such

[2] For convenience we defined with the scaled Wronskian with the current function $j_\pm(x,s)$ instead of the first derviative $\partial_x v_\pm(x,s)$, i.e. $W_s(x)/D$ would represent the standard definition of the Wronskian.

J. Stat. Mech. (2019) 024002

that $f_0(k) < 0$ holds in equation (29) with $\langle a|\psi_l^{\mathrm{R}}\rangle\langle\psi_l^{\mathrm{L}}|a\rangle \equiv \psi_l^{\mathrm{L}}(a)\psi_l^{\mathrm{R}}(a)$. Concurrently, the first passage weights follow from equation (31).

The formal backward duality from section 3.4, however, must be adopted as follows. After some tedious algebra we obtain formally the exact inverse duality in the form of

$$\tilde{P}(x,s|x_0) = \sigma_{\pm}\frac{\mathrm{e}^{\beta U(x_0)-\beta U(x)}\wp_{x_0}(s|x)}{D\frac{\partial}{\partial x_0}\ln[\wp_{x_0}(s|x)\wp_x(s|x_0)]}, \tag{40}$$

where sign $\sigma_{\pm} = -1$ if $x_0 < x$ and $\sigma_{\pm} = +1$ if $x_0 > x$; equation (40) can easily be verified by inserting the Wronskian (36) and the first passage time distribution (38) into the right hand side of equation (40), and comparing the result with the propagator from equation (37). Notably, this inverse duality is the continuous version of equation (34).

4.2. Relaxation under reflecting boundary conditions and strict spectral interlacing

In the previous subsection the target a divided the phase space into two regions, which implies that the first passage modes for the cases (I) and (II) separate into 'left' and 'right' modes as well. For example, if $x_1 < a$ and $x_2 > a$ one of the first passage weights $w_k(x_1)$ or $w_k(x_2)$ must typically be zero for all values of k. If one uses just the first M modes to approximate the propagator (see equation (39)) the zeros of the right hand side of

$$\tilde{P}^M(a,s|a) \equiv \sum_{k=0}^{M}\frac{\psi_k^{\mathrm{R}}(a)\psi_k^{\mathrm{L}}(a)}{s+\lambda_k}, \tag{41}$$

become approximations of the first passage modes and, hence, the weights $w_k^M(x_1)$ and $w_k^M(x_2)$ deduced from equation (41) will only satisfy $w_k^M(x_1) \ll w_k^M(x_2)$ (or $w_k^M(x_1) \gg w_k^M(x_2)$) for finite M, i.e. modes from case (I) and (II) mix. Such a mixing can be avoided entirely if the relaxation process is analyzed with a reflecting boundary at the target position a ($b_+ = a$ or $b_- = a$).

The result for reflecting boundary conditions $j_+(a) = 0$ (case (I)) and $j_-(a) = 0$ (case (II)) is automatically obtained by the following replacement:

$$\begin{aligned} v_{\pm}(x) &\to v_{\pm}(x,s)\,j_{\mp}(a,s) - j_{\pm}(a,s)v_{\mp}(x,s),\\ j_{\pm}(x) &\to j_{\pm}(x,s)\,j_{\mp}(a,s) - j_{\pm}(a,s)\,j_{\mp}(x,s), \end{aligned} \tag{42}$$

respectively, which inserted into the scaled Wronskian (36) at $x = a$ yields

$$W_s(a) = \begin{cases} v_+(a,s)\,j_-(a,s) & \text{if case (I) } x_0 < a,\\ -v_-(a,s)\,j_+(a,s) & \text{if case (II) } x_0 > a. \end{cases} \tag{43}$$

Utilizing the Wronskian for the reflecting boundary condition in equation (37) yields the diagonal of the propagator in the form

$$\tilde{P}(a,s|a) \equiv \lim_{\epsilon\to 0}\tilde{P}(a\pm\epsilon,s|a) = \pm\frac{v_{\pm}(a,s)}{j_{\pm}(a,s)}. \tag{44}$$

For two linearly independent functions $v_{\pm}$ with nonzero Wronskian (36) the zeros of $v_{\pm}$ and $j_{\pm}$ are different. Hence, the zeros of v_- in s contain only the first passage modes for

the case (I) $x_0 < a$, whereas the zeros of v_- do not contain zeros of first passage modes corresponding to the case (II) $x_0 > a$.

Let us from now on just focus on a case (I), in which $x_0 < a$, since case (II) follows by analogy. For case (I) we consider the Fokker–Planck operator $\mathbf{L}$ from equation (6) with zero current condition at $x = a$ and natural boundary condition for $x \to -\infty$. To that end we first determine the relaxation eigenvalues λ_k and eigenmodes $\psi_k^{\mathrm{R}}, \psi_k^{\mathrm{L}}$. Note that we consider the eigensystem in the presence of a reflecting wall. Without loss of generality we here explicitly treat only the 'left' problem $-\infty < x \leqslant a$, since the opposite 'right' problem (denoted later on with †) follows by analogy. As before we have the normalization $\int_{-\infty}^{a} \psi_k^{\mathrm{L}}(x)\psi_l^{\mathrm{R}}(x)\mathrm{d}x = \delta_{kl}$. Using $\{\psi_k^{\mathrm{L}}(x), \psi_l^{\mathrm{R}}(x)\}$ we now determine the first passage eigenvalues μ_k as explained in the previous subsection. The resulting first passage eigenvalues μ_k will automatically contain only first passage modes corresponding to the 'left' problem. This procedure remarkably simplifies the numerical determination of the first passage distribution, especially of those modes that are faster than the slowest mode of the 'right' problem (i.e. absorption from the right), $\mu_k > \mu_1^{\dagger}$, since a small number of modes M in equation (41) might otherwise be confused with 'fantom' modes from the opposite case †. In a related work [57] we investigated the 'left' first passage problem (case (I)) for a triple well potential in the presence of a reflecting boundary, and found an excellent agreement between the analytical first passage time distribution and computer simulations extending over many orders of magnitude in time using merely $M = 40$ relaxation modes. Finally, we have to point out that solving an eigenvalue problem $\{\lambda_k, \psi_k^{\mathrm{R}}\}$ with reflecting boundary condition is numerically easier than without reflecting boundary, i.e. natural boundaries albeit theoretically easier are numerically harder.

In the following section we apply these theoretical results to a discrete-state protein folding model and for the Ornstein–Uhlenbeck process.

5. Examples

5.1. Discrete protein folding model

We consider a simple continuous-time Markov state model for a protein with three structural elements as shown in figure 2. The protein starts from an initially unfolded state $x_0 = (0, 0, 0) \equiv \mathrm{I}$, from which it is searching for the native state $a = (1, 1, 1)$ through intermediate states II–VII (see e.g. [80, 81]). Each arrow in figure 2 indicates a possible transition $x \to x'$ $(x, x' = \mathrm{I}, \ldots, \mathrm{VIII},\ x \neq x')$ that occurs with a Arrhenius type rate $L(x', x) \equiv \exp(F_x - B_{xx'})$, where F_x denotes the free energy of state x and $B_{xx'} = B_{x'x}$ the energy barrier along the transition link $x \leftrightarrow x'$. The resulting transition matrix satisfies detailed balance $\ln[L(x', x)/L(x, x')] = F_x - F_{x'}$ for all values of $\{F_x, B_{xx'}\}$, and naturally has negative diagonal elements $L(x, x) = -\sum_{x' \neq x} L(x', x)$.

To test the power of the method from section 3.3 we set up the 8×8 transition matrix $\mathbf{L}$ with elements $\langle x'|\mathbf{L}|x\rangle = L(x', x)$ for a given set of energy barriers $B_{xx'}$ and free energies F_x. Then we carry out the eigendecomposition of $\mathbf{L}$, for which we first determine the eigenvalues $0 < \lambda_1, \ldots, \lambda_7$ (with $\lambda_0 = 0$) corresponding to the zeros of

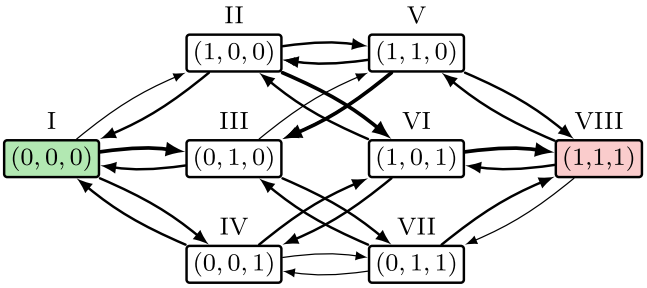

Figure 2. Discrete state protein folding model. Each arrow indicates a transition $x \to x'$ with rate $L(x', x) = \exp(F_x - B_{xx'})$, where $B_{xx'} = B_{x'x}$ is the energy barrier between the pair of states x and x' and F_x is the free energy of state x, where $x, x' = \mathrm{I}, \ldots, \mathrm{VIII}$. We randomly generated 100 folding landscapes with $B_{xx'}$ and F_x uniformly distributed within the interval $0 \leqslant B_{xx'}, F_x \leqslant 4$. The results for one particular realization of the landscape are presented in figure 3.

the characteristic function (16), $\chi(-\lambda_k) = 0$. We then determine the right eigenvectors $|\psi_k^{\mathrm{R}}\rangle$ by solving $\mathbf{L}|\psi_k^{\mathrm{R}}\rangle = -\lambda_k|\psi_k^{\mathrm{R}}\rangle$ for $k = 0, \ldots, 7$. The corresponding left eigenvectors, which solve $\langle\psi_k^{\mathrm{L}}|\mathbf{L} = -\langle\psi_k^{\mathrm{L}}|\lambda_k$, have components $\langle\psi_k^{\mathrm{L}}|x\rangle = \mathcal{N}^{-1}\mathrm{e}^{F_x}\langle x|\psi_k^{\mathrm{R}}\rangle$, where $\mathcal{N} = \sum_{x=\mathrm{I}}^{\mathrm{VIII}} \mathrm{e}^{F_x}|\langle\psi_k^{\mathrm{R}}|x\rangle|^2$ is a normalization factor. We take the function F_{k^*} as defined in equation (24), where $\Psi_k = \langle a|\psi_k^{\mathrm{R}}\rangle\langle\psi_k^{\mathrm{L}}|a\rangle$ and $\bar{\mu}_k = (\lambda_k + \lambda_{k-1})/2$ with $k = 0, \ldots, 7$, and choose $k^*(k) = k, k-1$ according to equation (26), which guarantees $f(s, k) = F_{k^*(k)}(s)$ to be negative at $s = -\bar{\mu}_k$. The truncated Newton series (27) involving the first N terms is then given by

$$\mu_k^N = \bar{\mu}_k + \sum_{n=1}^{N} \frac{f_0(k)^n}{f_1(k)^{2n-1}} \frac{\det \boldsymbol{\mathcal{A}}_n(k)}{(n-1)!}, \tag{45}$$

where $\det \boldsymbol{\mathcal{A}}_n(k)$ is the determinant of the almost triangular matrix from equation (28) and $f_i(k)$ is the ith derivative of $f(s, k)$ at $s = -\mu$, with explicit formulas given in equation (29). The weights $w_k(x_0)$ are determined using equation (31), i.e. by inserting $\mu_k \to \mu_k^N$. The calculations are performed for 100 randomly generated folding landscapes chosen as described in the caption to figure 2. In figure 3 we present the results for one particular realization of the folding landscape. Figure 3(a) displays the first passage time distribution for $N = 6$ and $N = 12$ on a doubly-logarithmic scale. The solid line represents the first passage time distribution obtained via a numerical diagonalization of $\mathbf{L}_a$. The corresponding duality solutions nicely overlap with the numerical result even on relatively short time scales (see inset for a plot with linear scales).

Having obtained the full distribution of first passage times is important for understanding kinetics in the so-called few encounter limit [48], in which for example 100 molecules are simultaneously searching for a state a. This scenario is indeed biologically relevant, for example, in the misfolding-triggered protein aggregation, which in turn leads to numerous diseases (see [57] for a more detailed discussion). Namely, as soon as the first protein molecule spontaneously misfolds it creates a nucleation site for further downhill misfolding and aggregation events ultimately leading to a macroscopic insoluble toxic aggregate.

In such a scenario the typical timescale of first arrivals will naturally be shifted towards shorter timescales, thus requiring an accurate determination of the full first

J. Stat. Mech. (2019) 024002

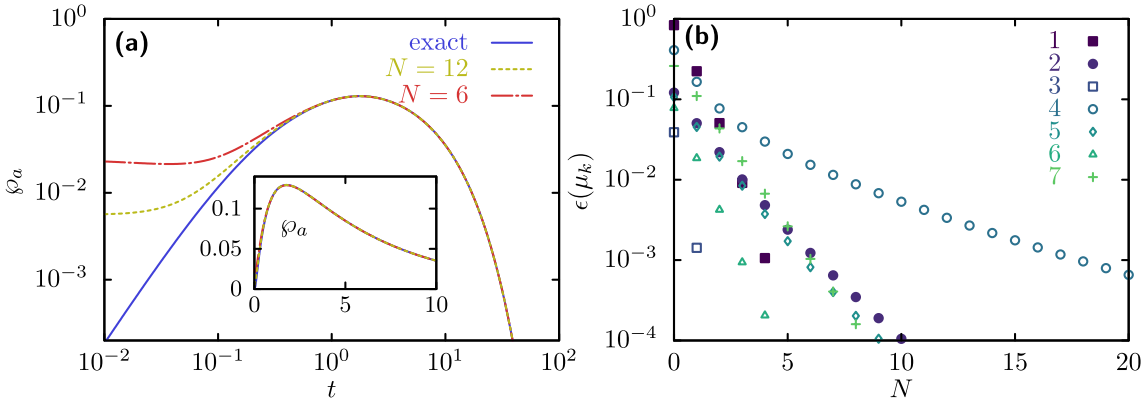

Figure 3. Results for a particular realization of the folding landscape. (a) First passage time distribution as function of time t. The Inset depicts the same data but on a linear time scale. (b) Relative error of the first passage eigenvalue $\epsilon(\mu_k) \equiv |\mu_{k,N} - \mu_k|/\mu_k$, where $\mu_{k,N}$ is the finite version of (27), where $n = 1, \ldots, N$.

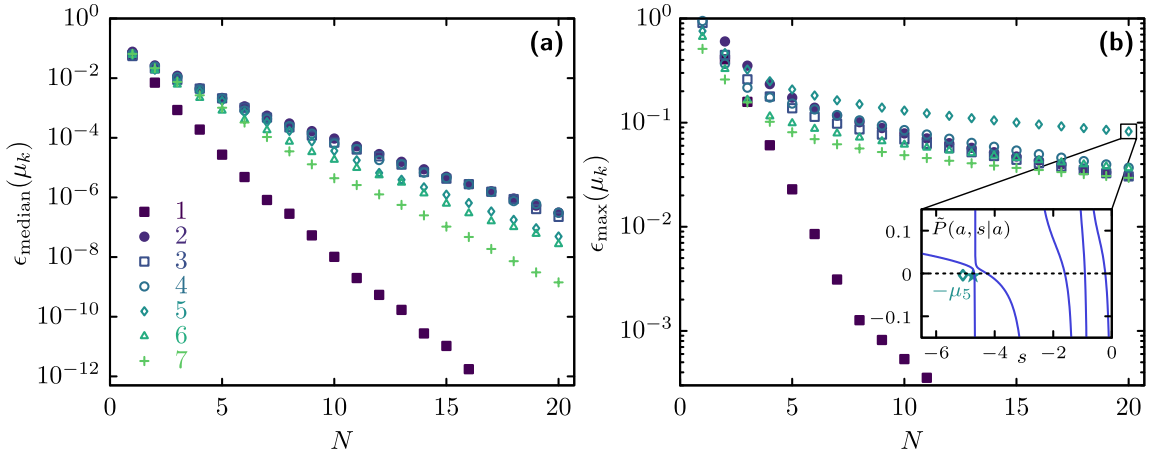

Figure 4. Rate of convergence of the truncated duality solution towards the respective numerical solution for randomly generated folding landscapes. We generated 100 folding landscapes according to figure 2 and determined for each model the error of the truncated Newton series (45) in terms of $\epsilon(\mu_k) \equiv |\mu_{k,N} - \mu_k|/\mu_k$ for all first passage eigenvalues $k = 1, 2, \ldots, 7$. (a) The typical error given by the median over all respective errors $\epsilon(\mu_k)$, as function of the number of terms N in the truncated Newton series (45). That is, 50 models generated a smaller error $\epsilon(\mu_k) \leqslant \epsilon_{\text{median}}(\mu_k)$ and 50 models generated a larger error $\epsilon(\mu_k) \geqslant \epsilon_{\text{median}}(\mu_k)$. (b) Maximal error $\epsilon(\mu_k) \equiv |\mu_{k,N} - \mu_k|/\mu_k$ out of all 100 randomly generated models as function of N. Here the maximal error (*worst case*) was observed for the fifth mode. The inset shows the diagonal of the propagator $\tilde{P}(a, s|a)$ as function of s for the model corresponding to the worst case; the approximations $-\mu_{k,N}$ for the corresponding first passage eigenvalue at $s = -\mu_5$ are indicated for $N = 20$ (diamond) and $N = 200$ (star).

J. Stat. Mech. (2019) 024002

passage statistics. Standard approaches focusing on the mean first passage time alone, would therefore fail in the few encounter limit, whereas our new framework provides an accurate and consistent result (see also [57] and figure 2 therein for more details).

In figure 4 we systematically analyze the deviation of the truncated Newton series (45) with respect to corresponding numerically obtained first passage eigenvalues μ_k for 100 randomly generated folding landscapes. For a given landscape the relative error is quantified in terms of the dimensionless quantity $\epsilon \equiv |\mu_k^N - \mu_k|/\mu_k$, and figure 4(a) depicts the typical error characterized by the median of the individual errors for all seven modes, respectively. Note that for $N = 20$ the relative error of the finite Newton series is typically below 10^{-6}.

Figure 4(b) displays the maximal error out of 100 randomly picked landscapes. We observe that larger errors can occur if a first passage eigenvalue is located immediately after a gap in the relaxation spectrum. The smaller error of the slowest first passage mode μ_1 is due to the fact that μ_1 cannot be located after such a gap due to the interlacing theorem (14), which implies $\mu_1 \leqslant \lambda_1$. In this specific example the maximum relative error out of 100 models randomly generated models is found for the fifth mode (μ_5); the inset of figure 4(b) shows the corresponding $\tilde{P}(a, s|a)$ as well as the result form the finite Newton series with $N = 20$ (see diamonds in the inset of figure 4(b)). In this extreme scenario the weight of the fifth relaxation mode $\Psi_5 \ll \Psi_{l\neq 5}$ is almost negligible compared to other weights, leading to an almost vanishing weight w_5, which would in turn require an increased number of terms N entering the Newton series. Increasing the number of terms in the truncated Newton series from $N = 20$ to $N = 200$ reduces the deviation from $\epsilon \simeq 10^{-1}$ to $\epsilon \simeq 10^{-2}$, the result for $N = 200$ is marked by the star in the inset of figure 4(b). Figure 4 readily demonstrates that the our duality can be robustly and reliably applied to all Markov state models.

5.2. Ornstein–Uhlenbeck process

Let us now consider a linear Ornstein–Uhlenbeck, which corresponds to a diffusion process in a harmonic potential $\beta U(x) = \omega x^2/2$. The corresponding Fokker–Planck operator reads $\mathbf{L} = D\partial_x \omega x + D\partial_x^2$. The eigendecomposition of the relaxation process in the absence of reflecting boundaries is well known. The respective eigenvalues are given by $\lambda_k = D\omega k$ with the corresponding eigenfunctions [72]

$$\begin{aligned}\psi_k^{\mathrm{R}}(x) &\equiv \langle x|\psi_k^{\mathrm{R}}\rangle = \frac{\mathrm{e}^{-\omega x^2/2}}{\sqrt{2\pi/\omega}}\frac{H_k(x\sqrt{\omega/2})}{k!2^k},\\ \psi_k^{\mathrm{L}}(x) &\equiv \langle \psi_k^{\mathrm{L}}|x\rangle = H_k(x\sqrt{\omega/2}),\end{aligned} \tag{46}$$

where H_k is the kth Hermite polynomial. Although this process is extremely well studied, a closed-form analytical result for the first passage time distribution $\wp_a(t|x_0)$ for any non-centered target position $a \neq 0$ remained elusive [82–84]. We note that the well known analytical solution of the Laplace transform of the probability density $\tilde{\wp}_a(s|x_0)$ in terms of Hermite polynomials [73, 82, 85, 86] until now could only be analytically inverted to $\wp_a(t|x_0)$ for the special case $a = 0$ [82]. Furthermore, the exact large deviation limit $\wp_a(t|x_0) \simeq w_1(x_0)\mathrm{e}^{-\mu_1 t}$ was just recently derived in [48]. To obtain the full first passage time distribution we here use equations (24)–(26) as follows. Inserting equation (46) into equations (24)–(26) yields the modifed diagonal of the propagator

J. Stat. Mech. (2019) 024002

$$f(s,k) = (s + D\omega k^*) \sum_{l=0}^{M} \frac{\mathrm{e}^{-\omega a^2/2}}{\sqrt{2\pi/\omega}} \frac{H_l(a\sqrt{\omega/2})^2}{l!2^l(s + D\omega l)} \tag{47}$$

where $k^*(k) = k,k-1$ is chosen according to equation (26), which is equivalent to $f(-\bar{\mu}_k, k) < 0$ with $\bar{\mu}_k = D\omega(k - 1/2)$. Note that we truncated the sum after M terms for the numerical evaluation, whereas the exact formal result corresponds to $M = \infty$. The first line of equation (29) is then simply given by $f_0(k) = f(-\bar{\mu}_k, k)$ and the second line of equation (29) becomes

$$f_{n\geqslant 1}(k) = \frac{\mathrm{e}^{-\omega a^2/2}}{(D\omega)^n\sqrt{2\pi/\omega}} \sum_{\substack{l=0 \\ l\neq k^*}}^{M} \frac{H_l(a\sqrt{\omega/2})^2(l-k^*)}{l!2^l(k-l-1/2)^{n+1}}. \tag{48}$$

The kth first passage eigenvalue μ_k is determined by using the finite Newton series (45), where the almost triangular matrix is taken from equation (28), and the corresponding first passage weights $w_k(x_0)$ are determined using the residue theorem (31). Note that our theory allows for the first time to determine analytically all first passage eigenvalues $\{\mu_k\}$ as well as the weights $\{w_k\}$ and, therefore, also provides a complete solution to the first passage time density $\wp_a(t|x_0)$.

Figure 5 depicts the results for the case, where the absorbing point is set at $a = 2$. Note that this scenario does not yet correspond to the well-known high barrier Kramers regime. In figure 5(a) we compare the exact $\tilde{P}(a, s|a)$ (solid blue line) with the finite approximation from equation (41) using $M = 20$ (dashed yellow line) and $M = 2000$ (dash-dotted red line) relaxation modes, respectively. The symbols represent the corresponding first passage modes ($s = -\mu_1, -\mu_2, \ldots$). Using only a small number of relaxation modes $M = 20$ (see yellow crosses) the zeros differ substantially from the respective numerically obtained solution, which becomes, however, rather well approximated if we increase the number of modes to $M = 2000$ (see open red circles). We note that such deviations of the first passage modes become particularly inconvenient for the modes that are marked by the vertical arrows in figure 5(a). These first passage modes correspond to an absorption from the right, where the corresponding weights vanish $w_k(x_0) = 0$ (here $k = 4, 7, 9, \ldots$) completely for all $x_0 \leqslant a$, which, however, is only obtained in the limit $M \to \infty$.

This numerical truncation problem can be avoided completely if the relaxation process is considered with a reflecting boundary condition as explained in section 4.2, which automatically removes beforehand all zeros marked by the arrows in figure 5(a) ($s = -\mu_4, -\mu_7, -\mu_9, \ldots$). Nevertheless, to illustrate the power and robustness of our duality approach we proceed here without a reflecting wall and use $M = 2000$. In figure 5(b) we show the first passage time distribution on a log-log scale (see inset for a linear scale) for three different starting positions $x_0 = 0,0.5,1$ (absorbing point $a = 2$). The lines represent the first passage time distribution which is determined using our new method (with $M = 2000$ relaxation modes) and the symbols represent the results $\wp_a$ of a numerical Laplace inversion of the renewal theorem (see figure caption for more details). We find a perfect agreement between our new analytical method (lines) and the numerical solution. For comparison, we imposed a reflecting wall at the target in a related article [57] and obtained a similarly excellent agreement between the duality solution and the simulated first passage time density using a total of $M = 40$ relaxation

J. Stat. Mech. (2019) 024002

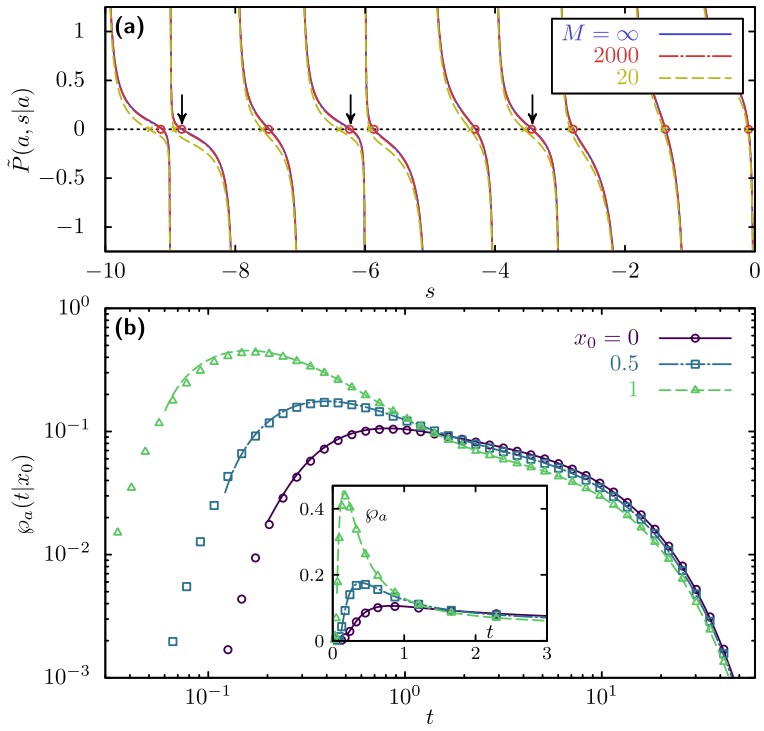

Figure 5. Analytical first passage time density for the Ornstein–Uhlenbeck process. (a) Exact diagonal of the relaxation propagator (solid blue line) versus a finite mode expansion $\tilde{P}(a,s|a) \approx \sum_k^M \Psi_k(a,a)/(s + D\omega k)$ for $M = 2000$ (dash-dotted red line) and $m = 20$ (dashed yellow line); the exact solution is obtained from (37) with particular solutions $v_\pm(a,s) = \mathrm{e}^{-\omega a^2/2} H_{-s/(D\omega)}(\pm a\sqrt{\omega/2})$, where $H_{-s}(x)$ is the generalized Hermite polynomial. The symbols represent the roots $s = -\mu_k$ that are determined from the Newton series (45) with $N = 10$ using $M = 2000$ (open red circles) and $M = 20$ (yellow crosses modes, respectively. The three vertical arrows $s = -\mu_k$ indicate the first passage eigenvalues that correspond to an absorption from the right, where $w_k(x_0) = 0$ for all $x_0 \leqslant a$. (b) First passage time distribution for three different initial conditions $x_0 = 0{,}0.5{,}1$. We have used $M = 2000$ relaxation modes and $N = 30$ and used our analytical forward duality to calculate the lines. The symbols represent a numerical inversion of the Laplace transform of $\tilde{\wp}_a(s|x_0) = \mathrm{e}^{\omega(a^2 - x_0^2)/2} H_{-s/(D\omega)}(-x_0\sqrt{\omega/2})/H_{-s/(D\omega)}(-a\sqrt{\omega/2})$ according to [82]. Parameters: $a = 2$, $\omega = D = 1$.

modes to quantify the first passage time statistics for diffusion in a multi-well potential. In either case, our new duality framework is exact for infinite M, and hence the desired precision can be tuned at will.

6. Concluding perspectives

We rigorously established a duality between the relaxation and the corresponding first passage processes in terms of an interlacing of eigenvalues. In other words, the time-scales at which a particle is absorbed into the target are proven to interlace with the

corresponding relaxation timescales. This duality allows us to understand first passage processes, both qualitatively and quantitatively, in terms of relaxation eigenmodes. For example, spectral gaps in the relaxation spectrum translate directly into spectral gaps in the first passage spectrum. More explicitly, in effectively one dimensional systems N gaps in the relaxation spectrum, arising from N local (free) energy basins, translate into $N-1$ gaps in the first passage time spectrum corresponding to the $N-1$ barriers separating the minima. Most importantly, we established a duality that allows, for the first time, to determine exactly the first passage time distribution from the corresponding relaxation spectrum.

Our theory is developed end tested on both, continuous reversible Fokker–Planck dynamics and Markov state jump processes in arbitrary dimensions. For convenience and without loss of generality, we restricted the applications of the duality for systems obeying Fokker–Planck dynamics to effectively one dimensional problems. An extension to more general models, for example, to diffusion on graphs would be straightforward, albeit rendering the calculations more cumbersome.

We tested and applied our theory to a discrete Markov state model of a simple protein folding landscape and the Ornstein–Uhlenbeck process, while a continuous analogue of a folding landscape are discussed elsewhere [57]. Notably, we have derived, to the best of our knowledge, for the first time an exact and explicit analytical expression for the first passage time distribution of the Ornstein–Uhlenbeck process.

Looking forward it will be interesting and relevant to apply the duality to the analysis of first passage processes on graphs. Applications of the duality to narrow escape problems in arbitrary dimensions [23–28] will also be carried out in future studies.

Finally, an extension of the framework to periodically or constantly driven systems (i.e. irreversible Markovian dynamics), which goes beyond the long time limit that is presented in the appendix, will be particularly challenging. Namely, there the interlacing theorem cannot be expected to hold anymore, since both eigenvalue spectra $\{\lambda_k\}$ and $\{\mu_k\}$ can become complex valued.

Acknowledgments

We thank Matteo Polettini for useful comments on our manuscript. The financial support from the German Research Foundation (DFG) through the Emmy Noether Program ‘GO 2762/1-1’ (to AG) is gratefully acknowledged.

Appendix. Explicit formula for principal eigenvalue

In this appendix we simplify equations (24)–(26) in the limit of a time-scale separation and for rare-event asymptotics for the principal first passage eigenvalue μ_1. We obtain a compact asymptotic expression of the principal first passage eigenvalue $\tilde{\mu}_1 \simeq \mu_1$, which is particular accurate if the time-scale of the slowest first passage eigenvalue is well separated from the time-scale of the slowest relaxation mode ($\mu_1 \ll \lambda_1$), which *inter alia* refines a previously proposed approximate link between the mean first passage time and the slowest relaxation mode [67, 68].

J. Stat. Mech. (2019) 024002

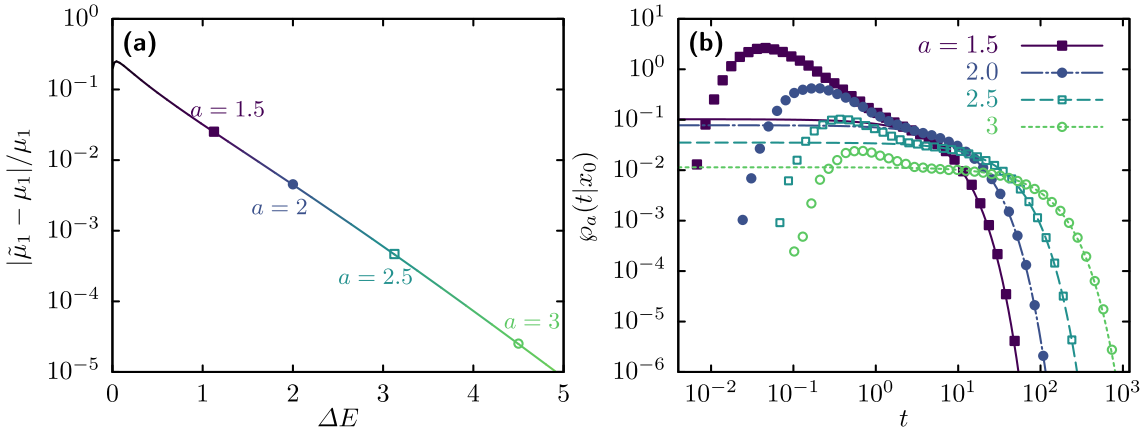

Figure A1. Principal eigenvalue for Ornstein–Uhlenbeck with potential $\beta U(x) = x^2/2$ (with $\omega = D = \beta = 1$). (a) Deviation of the approximation $\tilde{\mu}_1$ from the exact first passage eigenvalue μ_1 as function of the height of the energy barrier $\Delta E = a^2/2$. The symbols corresponds to the absorbing points $a = 1.5, 2, 2.5, 3$ used in (b). The colored solid line is calculated with equation (A.6). (b) First passage time density $\wp_a(t|x_0)$ for particle starting from $x_0 = 1$ as function of time t for target positions $a = 1.5, 2, 2.5, 3$. The lines correspond to long time limit approximation $\tilde{w}_1(x_0)\tilde{\mu}_1 \exp(\tilde{\mu}_1) \simeq \wp_a(t|x_0)$. The symbols represent $\wp_a(t|x_0)$ deduced from a histogram over 10^6 simulated trajectories. The weight $w_1(x_0)$ is deduced from the first line of equation (31), where μ_1 is replaced by $\tilde{\mu}_1$ and we have inserted the propagator from (37) with the solutions $v_\pm(x, s) = \mathrm{e}^{-x^2/2} H_s(\pm x/\sqrt{2})$.

First, we redefine equation (25) by setting $k = 1$, $k^* = 0$ and $\bar{\mu}_1 = 0$

$$f(s) = P_{\mathrm{eq}}(a) + \sum_{l \geqslant 1} \langle a|\psi_l^{\mathrm{R}}\rangle\langle\psi_l^{\mathrm{L}}|a\rangle \frac{s}{s + \lambda_l}, \tag{A.1}$$

where we dropped for convenience any argument with k since $k = 1$ is assumed throughout this appendix. The nth derivative of f at $s = 0$ simplifies with equation (29) to

$$f_n = \begin{cases} P_{\mathrm{eq}}(a) & \text{if } n = 0, \\ n!(-1)^{n+1} \sum_{l \geqslant 1} \langle a|\psi_l^{\mathrm{R}}\rangle\langle\psi_l^{\mathrm{L}}|a\rangle/\lambda_l^n & \text{if } n \geqslant 1. \end{cases} \tag{A.2}$$

The almost triangular matrices equation (28) become

$$\boldsymbol{\mathcal{A}}_n^{i,j} = \frac{f_{i-j+2}\Theta(i-j+1)}{(i-j+2)!}\Big[n(i-j+1)\Theta(j-2) + i\Theta(1-j) + j - 1\Big], \tag{A.3}$$

where we have replaced $f_n(k)$ by f_n from equation (A.2). Consequently, the Newton series (27) also simplifies to

$$\mu_1 = \sum_{n=1}^{\infty} \frac{f_0^n}{f_1^{2n-1}} \frac{\det \boldsymbol{\mathcal{A}}_n}{(n-1)!}. \tag{A.4}$$

If we now set $f_3 = f_4 = \ldots = 0$ in the almost triangular matrices (A.3), that is $\tilde{\boldsymbol{\mathcal{A}}}_n \equiv \boldsymbol{\mathcal{A}}_n|_{f_3 = f_4 = \ldots = 0}$, the resulting matrix $\tilde{\boldsymbol{\mathcal{A}}}_n$ becomes triangular, implying that its determinant is simply given by the product of the diagonal elements

J. Stat. Mech. (2019) 024002

$$\det \tilde{\boldsymbol{\mathcal{A}}}_n = \prod_{i=1}^{n-1} \boldsymbol{\mathcal{A}}_n^{i,i} = (f_2/2)^{n-1} \frac{(2n-2)!}{n!}, \tag{A.5}$$

where we have inserted equation (A.3) and evaluated the product in the last step. Replacing $\boldsymbol{\mathcal{A}} \to \tilde{\boldsymbol{\mathcal{A}}}_n$ in the Newton series (A.4) finally yields exactly

$$\tilde{\mu}_1 \equiv \sum_{n=1}^{\infty} \frac{f_0^n}{f_1^{2n-1}} \frac{\det \tilde{\boldsymbol{\mathcal{A}}}_n}{(n-1)!} = \frac{f_1 - \sqrt{f_1^2 - 2f_0 f_2}}{f_2}. \tag{A.6}$$

Equation (A.6) is nothing but the root of the second order Taylor expansion of $f(s)$ around $s = 0$ (i.e. the parabolic equation). This approximation is quite accurate whenever $\tilde{\mu}_1 \ll \lambda_1$.

If the target is located at a high energy barrier, such that slowest first passage eigenvalue is exponentially suppressed by the (free) energy at the target (i.e. $\mu_1 \propto \mathrm{e}^{-U(a)}$), equation (A.6) will lead to a quite accurate approximation $\tilde{\mu}_1$, which can be seen in figure A1. More precisely, in figure A1(a) we depict the relative error $|\tilde{\mu}_1 - \mu_1|/\mu_1$ as function of the target-site energy $\Delta E = a^2/2$ for the Ornstein–Uhlenbeck process from section 5.2 with $U(x) = x^2/2$ ($\omega = D = \beta = 1$). Conversely, figure A1(b) displays the results the first passage time distribution to four different target positions $a = 1.5, 2, 2.5, 3$ for a particle starting from $x_0 = 1$. The symbols represent histograms for $\wp_a(t|x_0)$ deduced from 10^6 Brownian dynamics trajectories, and the lines correspond to the large deviation asymptotic $\wp_a(t|x_0) \simeq w_1(x_0)\tilde{\mu}_1 \mathrm{e}^{-\tilde{\mu}_1 t}$ deduced from (A.6). We conclude that the limit $\mu_1 \ll \lambda_1$ lead to both, a quite accurate approximation $\tilde{\mu}_1 \simeq \mu_1$ and to an effectively single exponential decay $\mu_1 \ll \mu_2$ of the first passage statistics, which extends previous results [87] (see also [88]).

Moreover, a spectral gap such as $\lambda_1 \ll \lambda_2$ will also render $f_{n\geqslant 2}$ from equation (A.2) to be negligibly small if the target is not located at the global minimum of the potential. For example, a multi-barrier crossing, as the one studied in [57] (see figure 5 therein), the principal first passage eigenvalue from equation (A.6) deviates less than two percent from the exact value μ_1, i.e. $|\mu_1 - \tilde{\mu}_1|/\mu_1 < 0.02$. Notably, the approximation (A.6) refines previous conjectures that the mean first passage time to escape from the deepest potential basin corresponds to the first nonzero relaxation mode [67, 68].

We note that equation (A.6) can be reformulated to give

$$\tilde{\mu}_1 = \frac{\sigma_1}{2\sigma_2} \left[\sqrt{1 + 4\frac{P_{\mathrm{eq}}(a)\sigma_2}{\sigma_1^2}} - 1 \right], \tag{A.7}$$

where we inserted $f_0 = P_{\mathrm{eq}}(a)$ and defined $\sigma_n = \sum_{l\geqslant 1} \langle a|\psi_l^{\mathrm{R}}\rangle\langle\psi_l^{\mathrm{L}}|a\rangle/\lambda_l^n$. This relation is equivalent to equation (17) from a related article [57].

Finally, we emphasize that equations (A.4) and (A.6) apply also to homogeneous irreversible Markov processes, i.e. the relations from this appendix are not restricted to hold just for reversible Markov chains.

References

[1] Kramers H 1940 Brownian motion in a field of force and the diffusion model of chemical reactions *Physica* **7** 284–304

J. Stat. Mech. (2019) 024002

[2] Szabo A, Schulten K and Schulten Z 1980 First passage time approach to diffusion controlled reactions *J. Chem. Phys.* **72** 4350–7
[3] Ben-Naim E, Redner S and Leyvraz F 1993 Decay kinetics of ballistic annihilation *Phys. Rev. Lett.* **70** 1890–3
[4] Oshanin G, Stemmer A, Luding S and Blumen A 1995 Smoluchowski approach for three-body reactions in one dimension *Phys. Rev.* E **52** 5800–5
[5] Mejía-Monasterio C, Oshanin G and Schehr G 2011 First passages for a search by a swarm of independent random searchers *J. Stat. Mech.* P06022
[6] Guérin T, Levernier N, Bénichou O and Voituriez R 2016 Mean first-passage times of non-Markovian random walkers in confinement *Nature* **534** 356–9
[7] Li Y, Debnath D, Ghosh P K and Marchesoni F 2017 Nonlocality of relaxation rates in disordered landscapes *J. Chem. Phys.* **146** 084104
[8] Hänggi P, Talkner P and Borkovec M 1990 Reaction-rate theory: fifty years after Kramers *Rev. Mod. Phys.* **62** 251–341
[9] Redner S 2001 *A Guide to First-Passage Processes* (Cambridge: Cambridge University Press)
[10] Metzler R, Oshanin G and Redner S (ed) 2014 *First-Passage Phenomena and their Applications* (Singapore: World Scientific)
[11] Bénichou O and Voituriez R 2014 From first-passage times of random walks in confinement to geometry-controlled kinetics *Phys. Rep.* **539** 225–84
[12] Kopelman R 1988 Fractal reaction kinetics *Science* **241** 1620–6
[13] ben Avraham D and Havlin S 2000 *Diffusion and Reactions in Fractals and Disordered Systems* (Cambridge: Cambridge University Press)
[14] Rupprecht J-F, Bénichou O, Grebenkov D S and Voituriez R 2015 Exit time distribution in spherically symmetric two-dimensional domains *J. Stat. Phys.* **158** 192–230
[15] Grebenkov D S 2016 Universal formula for the mean first passage time in planar domains *Phys. Rev. Lett.* **117** 260201
[16] Bressloff P C and Newby J M 2013 Stochastic models of intracellular transport *Rev. Mod. Phys.* **85** 135–96
[17] Godec A and Metzler R 2015 Optimization and universality of Brownian search in a basic model of quenched heterogeneous media *Phys. Rev.* E **91** 052134
[18] Vaccario G, Antoine C and Talbot J 2015 First-passage times in d-dimensional heterogeneous media *Phys. Rev. Lett.* **115** 240601
[19] Godec A and Metzler R 2016 First passage time distribution in heterogeneity controlled kinetics: going beyond the mean first passage time *Sci. Rep.* **6** 20349
[20] Vilela R D and Lindner B 2009 Comparative study of different integrate-and-fire neurons: spontaneous activity, dynamical response and stimulus-induced correlation *Phys. Rev.* E **80** 031909
[21] Braun W, Matthews P C and Thul R 2015 First-passage times in integrate-and-fire neurons with stochastic thresholds *Phys. Rev.* E **91** 052701
[22] Barkai E, Aghion E and Kessler D A 2014 From the area under the Bessel excursion to anomalous diffusion of cold atoms *Phys. Rev.* X **4** 021036
[23] Singer A, Schuss Z and Holcman D 2006 Narrow escape, part ii: the circular disk *J. Stat. Phys.* **122** 465–89
[24] Schuss Z, Singer A and Holcman D 2007 The narrow escape problem for diffusion in cellular microdomains *Proc. Natl Acad. Sci. USA* **104** 16098–103
[25] Reingruber J and Holcman D 2009 Gated narrow escape time for molecular signaling *Phys. Rev. Lett.* **103** 148102
[26] Pillay S, Ward M J, Peirce A and Kolokolnikov T 2010 An asymptotic analysis of the mean first passage time for narrow escape problems: part I: two-dimensional domains *Multiscale Model. Simul.* **8** 803–35
[27] Isaacson S A, Mauro A J and Newby J 2016 Uniform asymptotic approximation of diffusion to a small target: Generalized reaction models *Phys. Rev.* E **94** 042414
[28] Grebenkov D S and Oshanin G 2017 Diffusive escape through a narrow opening: new insights into a classic problem *Phys. Chem. Chem. Phys.* **19** 2723–39
[29] Palyulin V V, Chechkin A V and Metzler R 2014 Lévy flights do not always optimize random blind search for sparse targets *Proc. Natl Acad. Sci. USA* **111** 2931–6
[30] Godec A and Metzler R 2017 First passage time statistics for two-channel diffusion *J. Phys. A: Math. Theor.* **50** 084001
[31] Bénichou O, Loverdo C, Moreau M and Voituriez R 2011 Intermittent search strategies *Rev. Mod. Phys.* **83** 81–129
[32] Majumdar S N and Bray A J 2001 Spatial persistence of fluctuating interfaces *Phys. Rev. Lett.* **86** 3700–3
[33] Majumdar S N and Comtet A 2002 Exact asymptotic results for persistence in the Sinai model with arbitrary drift *Phys. Rev.* E **66** 061105

J. Stat. Mech. (2019) 024002

[34] Bray A J, Majumdar S N and Schehr G 2013 Persistence and first-passage properties in nonequilibrium systems *Adv. Phys.* **62** 225–361
[35] Jarzynski C 2011 Equalities and inequalities: irreversibility and the second law of thermodynamics at the nanoscale *Annu. Rev. Condens. Matter Phys.* **2** 329–51
[36] Seifert U 2012 Stochastic thermodynamics, fluctuation theorems and molecular machines *Rep. Prog. Phys.* **75** 126001
[37] Van den Broeck C and Esposito M 2015 Ensemble and trajectory thermodynamics: a brief introduction *Physica* A **418** 6–16
[38] Neri I, Roldán É and Jülicher F 2017 Statistics of infima and stopping times of entropy production and applications to active molecular processes *Phys. Rev.* X **7** 011019
[39] Fuchs J, Goldt S and Seifert U 2016 Stochastic thermodynamics of resetting *Europhys. Lett.* **113** 60009
[40] Roldán É and Gupta S 2017 Path-integral formalism for stochastic resetting: exactly solved examples and shortcuts to confinement *Phys. Rev.* E **96** 022130
[41] Garrahan J P 2017 Simple bounds on fluctuations and uncertainty relations for first-passage times of counting observables *Phys. Rev.* E **95** 032134
[42] Gingrich T R and Horowitz J M 2017 Fundamental bounds on first passage time fluctuations for currents *Phys. Rev. Lett.* **119** 170601
[43] Barato A C and Seifert U 2015 Thermodynamic uncertainty relation for biomolecular processes *Phys. Rev. Lett.* **114** 158101
[44] Kolesov G, Wunderlich Z, Laikova O N, Gelfand M S and Mirny L A 2007 How gene order is influenced by the biophysics of transcription regulation *Proc. Natl Acad. Sci. USA* **104** 13948–53
[45] Fraser P and Bickmore W 2007 Nuclear organization of the genome and the potential for gene regulation *Nature* **447** 413–7
[46] Bénichou O, Chevalier C, Klafter J, Meyer B and Voituriez R 2010 Geometry-controlled kinetics *Nat. Chem.* **2** 472–7
[47] Meyer B, Chevalier C, Voituriez R and Bénichou O 2011 Universality classes of first-passage-time distribution in confined media *Phys. Rev.* E **83** 051116
[48] Godec A and Metzler R 2016 Universal proximity effect in target search kinetics in the few-encounter limit *Phys. Rev.* X **6** 041037
[49] Bialek W 2012 *Biophysics: Searching for Principles* (Princeton, NJ: Princeton University Press)
[50] Pulkkinen O and Metzler R 2013 Distance matters: the impact of gene proximity in bacterial gene regulation *Phys. Rev. Lett.* **110** 198101
[51] Dobson C M 2003 Protein folding and misfolding *Nature* **426** 884–90
[52] Chiti F and Dobson C M 2006 Protein misfolding, functional amyloid and human disease *Annu. Rev. Biochem.* **75** 333–66
[53] Zheng W, Schafer N P and Wolynes P G 2013 Free energy landscapes for initiation and branching of protein aggregation *Proc. Natl Acad. Sci. USA* **110** 20515–20
[54] Yu H, Dee D R, Liu X, Brigley A M, Sosova I and Woodside M T 2015 Protein misfolding occurs by slow diffusion across multiple barriers in a rough energy landscape *Proc. Natl Acad. Sci. USA* **112** 8308–13
[55] Dee D R and Woodside M T 2016 Comparing the energy landscapes for native folding and aggregation of PrP *Prion* **10** 207–20
[56] Nguyen B, Hartich D, Seifert U and De Los Rios P 2017 Thermodynamic bounds on the ultra- and infra-affinity of Hsp70 for its substrates *Biophys. J.* **113** 362–70
[57] Hartich D and Godec A 2018 Duality between relaxation and first passage in reversible Markov dynamics: rugged energy landscapes disentangled *New J. Phys.* **20** 112002
[58] Schnoerr D, Sanguinetti G and Grima R 2017 Approximation and inference methods for stochastic biochemical kinetics—a tutorial review *J. Phys. A: Math. Theor.* **50** 093001
[59] Munsky B, Nemenman I and Bel G 2009 Specificity and completion time distributions of biochemical processes *J. Chem. Phys.* **131** 235103
[60] Bel G, Munsky B and Nemenman I 2010 The simplicity of completion time distributions for common complex biochemical processes *Phys. Biol.* **7** 016003
[61] Grima R and Leier A 2017 Exact product formation rates for stochastic enzyme kinetics *J. Phys. Chem.* B **121** 13–23
[62] Schnoerr D, Cseke B, Grima R and Sanguinetti G 2017 Efficient low-order approximation of first-passage time distributions *Phys. Rev. Lett.* **119** 210601
[63] Weber M F and Frey E 2017 Master equations and the theory of stochastic path integrals *Rep. Prog. Phys.* **80** 046601
[64] Biroli G and Kurchan J 2001 Metastable states in glassy systems *Phys. Rev.* E **64** 016101

J. Stat. Mech. (2019) 024002

[65] Tănase-Nicola S and Kurchan J 2003 Topological methods for searching barriers and reaction paths *Phys. Rev. Lett.* **91** 188302
[66] Tănase-Nicola S and Kurchan J 2004 Metastable states, transitions, basins and borders at finite temperatures *J. Stat. Phys.* **116** 1201–45
[67] Schuss Z and Matkowsky B J 1979 The exit problem: a new approach to diffusion across potential barriers *SIAM J. Appl. Math.* **36** 604–23
[68] Matkowsky B J and Schuss Z 1981 Eigenvalues of the Fokker–Planck operator and the approach to equilibrium for diffusions in potential fields *SIAM J. Appl. Math.* **40** 242–54
[69] Grone R, Hoffmann K H and Salamon P 2008 An interlacing theorem for reversible Markov chains *J. Phys. A: Math. Theor.* **41** 212002
[70] van Kampen N G 2007 *Stochastic Processes in Physics and Chemistry* (*North-Holland Personal Library*) 3rd edn (Amsterdam: Elsevier)
[71] Kadanoff L P and Swift J 1968 Transport coefficients near the critical point: a master-equation approach *Phys. Rev.* **165** 310–22
[72] Gardiner C W 2004 *Handbook of Stochastic Methods* 3rd edn (Berlin: Springer)
[73] Siegert A J F 1951 On the first passage time probability problem *Phys. Rev.* **81** 617–23
[74] Polettini M and Esposito M 2017 Effective thermodynamics for a marginal observer *Phys. Rev. Lett.* **119** 240601
[75] Bisker G, Polettini M, Gingrich T R and Horowitz J M 2017 Hierarchical bounds on entropy production inferred from partial information *J. Stat. Mech.* 093210
[76] Keilson J 1964 A review of transient behavior in regular diffusion and birth-death processes *J. Appl. Prob.* **1** 247–66
[77] Cahill N D, D'Errico J R, Narayan D A and Narayan J Y 2002 Fibonacci determinants *Coll. Math. J.* **33** 221–5
[78] Jia J-T 2018 Numerical algorithms for the determinant evaluation of general Hessenberg matrices *J. Math. Chem.* **56** 247–56
[79] Titchmarsh E C 1962 *Eigenfunction Expansions Associated with Second-Order Differential Equation* 2nd edn (London: Oxford University Press)
[80] Prinz J-H, Keller B and Noé F 2011 Probing molecular kinetics with Markov models: metastable states, transition pathways and spectroscopic observables *Phys. Chem. Chem. Phys.* **13** 16912–27
[81] Bowman G R, Pande V S and Noé F (ed) 2014 *An Introduction to Markov State Models and their Application to Long Timescale Molecular Simulation* (Dordrecht: Springer)
[82] Alili L, Patie P and Pedersen J L 2005 Representations of the first hitting time density of an Ornstein–Uhlenbeck process *Stoch. Models* **21** 967–80
[83] Grebenkov D S 2015 First exit times of harmonically trapped particles: a didactic review *J. Phys. A: Math. Theor.* **48** 013001
[84] Nyberg M, Ambjörnsson T and Lizana L 2016 A simple method to calculate first-passage time densities with arbitrary initial conditions *New J. Phys.* **18** 063019
[85] Darling D A and Siegert A J F 1953 The first passage problem for a continuous Markov process *Ann. Math. Stat.* **24** 624–39
[86] Vergassola M, Deneke V E and Di Talia S 2018 Mitotic waves in the early embryogenesis of Drosophila: bistability traded for speed *Proc. Natl Acad. Sci. USA* **115** E2165
[87] Berezhkovskii A and Szabo A 2004 Ensemble of transition states for two-state protein folding from the eigenvectors of rate matrices *J. Chem. Phys.* **121** 9186
[88] Bicout D J and Szabo A 2000 Entropic barriers, transition states, funnels and exponential protein folding kinetics: a simple model *Protein Sci.* **9** 452–65

J. Stat. Mech. (2019) 024002